A master regulatory network restoring brain glutamate homeostasis is coordinately activated in stroke

Mariko Kobayashi[1,3], Corey Anderson[2], Corinne Benakis[2], Michael J. Moore[1], Aldo Mele[1], John J. Fak[1], Christopher Y. Park[1], Ping Zhou[2], Josef Anrather[2], Costantino Iadecola[2], Robert B. Darnell[1,3].

[1]Laboratory of Molecular Neuro-Oncology and Howard Hughes Medical Institute, The Rockefeller University, 1230 York Avenue, New York, NY 10065, USA. [2]Fell Family Brain and Mind Research Institute, Weill Cornell Medicine, 407 East 61st Street, New York, NY, 10065, USA.

[3]Correspondence: mkobayashi@rockefeller.edu, darnelr@rockefeller.edu

ABSTRACT

Altered miRNA expression in various disease states have been identified, but their global targets contributing to the collective regulatory power to promote or attenuate pathology remains poorly defined. Here we applied a combination of hi-throughput RNA profiling techniques, including AGO CLIP, miRNAseq, RNAseq and ribosomal profiling, to develop an unbiased and comprehensive view of miRNA:mRNA functional interactions following ischemia/reperfusion (IR) injury in the mouse brain. Upon acute I/R insult miR-29 family members were most prominently lost, with corresponding de-regulation of their global target sites. This leads to a dynamic, cascading mode of miR-29 target transcript activation, orchestrated by an initial translational activation and subsequent increase in target mRNA levels. Unexpectedly, activated genes include factors essential for glutamate signaling and re-uptake, indicating a fundamental role for this regulatory network in modulating critical endogenous neuroprotective programs to restore brain homeostasis. We integrated this data with human brain AGO CLIP profiles to infer target site variants that determine miRNA binding and to explore the role of non-coding site polymorphisms in stroke. Together these results establish a new strategy for understanding RNA regulatory networks in complex neurological disease.

INTRODUCTION

Divergent post-transcriptional gene regulation in the brain is indispensable to achieve its highly specialized and diverse functions. An aspect of this control is mediated by miRNAs, small non-coding RNAs that fine-tune gene expression by base pairing to mRNAs' 3' ends (Baek et al., 2008; Bartel, 2009). A single miRNA can have multiple targets, providing coordinate governance over a network of genes. Their dynamic regulatory capacity, including precise temporal responses to external cues (Ebert and Sharp, 2012) and spatial-specific targeting of localized mRNAs (Leung and Sharp, 2006) provide an elegant molecular solution to meet the brain's unique physiological demands. Ablation of the miRNA processing machinery, *Dicer*, leads to neuronal loss, memory/behavior deficits, neurodegenerative phenotypes akin to Parkinson's Disease (PD) and even enhancement of poly-glutamine toxicity (Bilen et al., 2006; Kim et al., 2007; Davis et al., 2008). Although substantial research has determined a requirement of miRNAs for proper function, the identities, targets, and collective roles of their regulatory network in disease remain largely unknown.

The development of high-throughput approaches to capture and identify cellular RNAs has catapulted the search for miRNA master regulatory networks. These unbiased, highly sensitive

and quantitative technologies have been especially useful for identifying miRNA with divergent expression patterns in a given disease (Kim et al., 2007, Minones-Moyano et al., 2011, However, despite expanding our knowledge database, these studies are limited by their inability to define precise gene regulatory networks impacted from varying miRNA expression levels. HITS-CLIP combines rigorous biochemical methods with hi-throughput sequencing technology to identify bona fide RNA:protein interactions (Licatalosi et al., 2008). When applied with RNA-induced silencing complex (RISC) factor Argonaute (AGO), AGO HITS-CLIP allows for empirical mapping of miRNA targeting events through isolation of endogenous AGO:miRNA:mRNA (ternary) complexes (Chi et al., 2009, Moore et al., 2014). Application of AGO HITS-CLIP was instrumental for the discovery of novel miRNA mechanisms in unique biological contexts, including coordinate control of viral latency, viral sequestration of host miRNAs, viral genome propagation by 3'UTR targeting (Riley et al., 2012; Luna et al., 2015; Scheel et al., 2016), and cell invasion networks in cancer (Bracken et al., 2014). Recent modification of CLIP (CLEAR-CLIP) utilizes covalent ligation of RNAs within AGO ternary complexes to garner miRNA-target chimeras for the precise identification of *in vivo* miRNA targeting events in mammalian tissues (Moore et al., 2015). Also, similar approaches using exogenous AGO expression have been used to study AGO complexes in model organisms (Helwak et al., 2013, Grosswendt et al., 2014). These methods provide powerful tools to facilitate genome-wide discovery of miRNA function in disease with potential to uncover new targets for therapy.

Here, we employed AGO HITS-CLIP for transcriptome-wide mapping of altered miRNA targeting events in an I/R injury model of stroke. Differential profiling of AGO bound RNA distinguished over one thousand miRNA:mRNA events changing in response to stroke. Detailing the global molecular events lead by a single family of robustly down-regulated miRNAs, miR-29s, unveiled a coordinate cascade of target gene activation mediating a dynamic, endogenous neuroprotective responses to I/R brain injury. Unexpectedly, many of the functional miRNA binding events relied on non-canonical seed pairing events, underscoring the importance of empirically identified targets over informatic predictions. Moreover, stroke miRNAs impacted mRNA translation as an early event, prior to effects on steady state levels of mRNA targets. We extend these findings to provide new insights to the regulation of specific protein targets impacted in stroke, and to regulatory site polymorphisms as potential determinants of disease outcome. Collectively, our approach reveals a transcriptome-wide regulation of a miRNA network acutely altered in I/R brain injury and merge empirical findings in an animal model with human genetics to introduce a novel strategy toward understanding human stroke disease.

RESULTS

Identification of AGO:RNA interactions in stroke response

To model human ischemic stroke, we used the mouse middle cerebral artery occlusion (MCAO) model (Figure 1A). This procedure relies on the transient occlusion of the middle cerebral artery (MCA), the artery most often occluded in stroke patients, and further model the molecular events of reperfusion that follow (Casals et al., 2011, Jackman et al., 2011). We chose an early time point of 3hrs (post I/R injury) in order to distinguish direct molecular consequences of stroke injury from indirect events involving secondary phenomena such as major cell death and infiltration of blood-borne inflammatory cells (Iadecola and Anrather, 2011).

For differential analysis of AGO-associated RNA, we compared data from 'Stroke' hemisphere, containing the ischemic territory, to the contralateral or 'Control' hemisphere (Figure 1A). Sham surgery animals were also assessed to rule out general affects caused by surgical anesthesia (Figure S1A). We focused our biochemical analysis on cortical tissues surrounding the center of the ischemic territory (ischemic core), and including the "ischemic penumbra," a region at risk for infarction targeted by intrinsic neuro-protective mechanisms (Figure 1A, Kunz et al, 2007, Iadecola and Anrather, 2011). The AGO CLIP protocol on these samples was executed as previously described (Chi et al., 2009, Moore et al., 2014) (Figure 1B), using stringent methods to isolate UV-crosslinked AGO:RNA complexes by immunoprecipitation and gel purification. Autoradiograms of cross-linked RNAs revealed no difference in the amount of purified complexes in the stroke samples with respect to controls (Figure S1B). The isolated AGO-bound mRNAs and miRNAs were sequenced using high-throughput sequencing platforms and mapped to the mouse reference genome for peak definition, using a previously reported peak calling strategy (Chi et al., 2009, Moore et al., 2014), and to the miRBase reference of miRNAs (Kozomara and Griffiths-Jones, 2010).

Differential bioinformatic analysis of mapped sites was performed to reveal stroke-specific AGO binding patterns (Figure 1B). CLIP sequencing reads across 4-5 biological replicates had high correlations (average Pearson correlation coefficients of ~0.7 to 0.9 for CLIP'd miRNAs, and ~0.6 for CLIP'd mRNAs (Figure S1C-D). Differential analysis of binding events reproducible in at least 3 replicates (biological complexity, BC3 or greater) (Moore et al., 2014) identified 123 miRNAs with altered AGO association in stroke, of which 61 showed a significant increase while 62 showed a significant decrease (Figure 1C, Supplementary Table 1). The most notable changes in AGO-bound miRNAs were observed with all three members of the miR-29 family, miR-29a, -29b, -29c, each significantly reduced in AGO binding in stroke (Figure 1C). Difference analysis of the two negative controls, 'Sham' and 'Control,' demonstrated minimal resemblance to 'Stroke' comparison (Figure S1E).

For the investigation of AGO-CLIP mRNAs, identified peaks were assigned to AGO footprints of 80 nt relative to peak midpoints, slightly wider than previously defined peak width (Chi et al., 2009), in order to balance the peak widths across all reproducible binding events. Only peaks containing tags from 3 out of 5 biological replicates were considered (BC≥3). Using this approach, we identified 18,285 reproducible AGO peaks, out of which 1,190 were differentially bound by AGO in stroke condition (determined by binomial testing and applying p-value cut off of $p < 0.05$). Among these 'stroke peaks', 430 showed increased binding while 760 showed a significant decrease (Figure 1D, Supplementary Table 1). Although canonical miRNA targeting is at the 3'UTRs of mRNAs, previous AGO-CLIP studies have shown miRNA guided AGO binding also occurs within coding sequences, 5'UTRs and in introns of mRNAs (Chi et al., 2009, Moore et al., 2014). To assess whether the transcriptome-wide location of AGO targeting is altered in stroke brain, we determined the distribution of 1,190 stroke-associated peaks among annotated transcript regions. As expected, the majority (45%) of AGO regulated sites in stroke were identified within annotated 3'UTR regions, with smaller fractions residing in introns (29%) and in coding sequences (18%). Additionally, we saw no difference in the distribution of stroke peaks among transcript locations against 'all' AGO binding events (Figure 1E). The proportion of 3'UTR peaks was even higher (49%) when indeterminate peaks, also found in 'Sham' vs 'Control comparisons, were filtered out (Figure S1F-G). Finally, we performed a 6-nucleotide motif enrichment analysis of altered peaks ($p<0.05$) in 3'UTRs to identify associated miRNAs (Figure 1F). Among AGO binding events up-regulated in stroke, we found seed matched sequences of miR-3112, -135ab, -669f, -743ab, -466f, and -34abc. The top motifs enriched in down-regulated peaks were seed matches of miR-29abc, -667*, -

149, -466bc, -181b, and -291ab, many of which have been previously implicated in stroke (Jeyaseelan et al., 2008a, Dharap et al., 2009, Liu et al., 2015, Liu et al., 2009). Since our primary interest was to identify activated targets of miRNA regulation, we emphasized on down-regulated miRNAs for this study.

miR-29 family of miRNAs are down-regulated in stroke

AGO HITS-CLIP data showed members of miR-29 family were all robustly altered, and unanimously down-regulated in I/R injury (Fig1C, 1F). To confirm this we used an orthogonal approach, measuring mature miRNA levels using small RNA sequencing. Although the global correlation of changes in AGO-bound miRNAs and steady-state level changes was poor (Pearson correlation coefficient = -0.1), the assessment showed the loss of AGO facilitated miR-29 regulation was due to a reduction in mature miRNA levels (Figure 2A, S2, Supplementary Table 2). This was further corroborated by qPCR quantification of each miR-29 family member (Figure 2B). Additionally, the loss of miR-29 was not detected in the sham surgery condition (Figure 2B, S2A), ruling out confounding effects of general anesthesia and surgical manipulation. Next, we determined if AGO binding to miR-29 targets are also lost at 3 hours after I/R. To define cognate miR-29 sites in our data, we examined stroke altered peaks with TargetScan (Lewis et al., 2005; Grimson et al., 2007) and more precisely with empirically identified sites by brain CLEAR-CLIP (Moore et al., 2015). This network of miR-29 targets was assessed for AGO binding changes in stroke versus control brain. Cumulative distribution function (CDF) plots of fold changes in CLIP showed a significant global reduction in AGO binding to the miR-29 targets. This was observed relative to a number of controls, including AGO binding to the targets of the top 10 brain most abundant miRNAs and to let-7 targets (Figure 2C). CLIP fold changes between sham surgery and control comparison for miR-29 targets showed no difference to those of control miRNAs, suggesting down-regulation of miR-29 targets is specific to I/R injury (Figure 2D). Collectively, these data demonstrate a loss of miR-29 targeting of its regulatory network following I/R injury.

Acute de-repression of miR-29 targets occurs mainly by translational activation

To assess the functional consequences resulting from the loss of AGO-miR-29 targeting in acute I/R injury response, we considered whether the relief in miR-29 repression after stroke occurred by stabilizing target mRNAs or by activating their translation (Bartel, 2009). Surprisingly, RNAseq analysis of miR-29 target mRNA levels did not show noticeable changes in stroke conditions with respect to genes targeted by other miRNAs (*ie*. let-7) (Figure 3A). This was unexpected, as mechanistic studies using global approaches report miRNAs act mainly through deadenylation and mRNA decay (Guo et al., 2010; Eichhorn et al., 2014), and thus hypothesized miRNA loss will result in transcript stabilization. We next examined translational effects corresponding to the loss of AGO-miR-29 targeting, using a modified ribosomal profiling (RPF) approach (Ingolia et al., 2009) (Figure S3A) to quantify ribosome protected mRNA fragments in I/R injured brain. Stroke or control brain cortex (3hr post I/R) was treated with cycloheximide to stabilize ribosomes on translating RNAs. Following nuclease digestion, 80S monosomes were fractionated on sucrose gradients, further purified by immunoprecipitation using antibodies specific to the large ribosomal subunit, and monosome-associated mRNA tags cloned and analyzed by high-throughput sequencing. We saw no alterations in the amount of available monosomes, distribution of monosome-associated tags in stroke condition relative to controls, or RPF tag coverage across start and stop codons (Figure S3B-E). In contrast, differential analysis of stroke RPF footprint densities revealed over 400 transcripts with significant changes in ribosome association (Figure S3F, Supplementary Table 3), many without detectable changes in mRNA levels (Figure 3B).

These results suggested that in the acute regulatory environment of I/R injury, translational regulation dominates mRNA stability in determining physiological outcomes. Indeed, analysis of RPF fold change distribution of miR-29 targets showed a robust increase relative to the entire translatome, whereas control transcripts (the targets of let-7 or of the top-10 expressed brain miRNAs) did not (Figure 3C). Furthermore, calculating translational efficiency (TE), or the ratio of ribosome footprint density to mRNA abundance (Ingolia et al., 2009), showed even greater activation among miR-29 targets (Figure 3E). This observation was specific to stroke and not influenced by general surgery procedures, as comparison between sham and control revealed insignificant differences (Figure 3D, 3F). Taken together these data reveal translational activation is the predominant functional consequence of miR-29 loss and hence a distinct mechanism of miRNA target activation in I/R brain injury, and further suggest a role for activated miR-29 targets in facilitating coordinated responses of neuro-protection and cell death.

RNA levels of miR-29 targets increase at later times following stroke

The cellular response to I/R injury is a complicated and dynamic process, involving many factors that generate influence at various times. Moreover, miRNAs mediating this process are highly variable, their expression and physiological impact are likely to rely on duration of ischemia, severity of injury, and time after reperfusion (Kalogeris et al., 2012). We asked whether the down-regulation of miR-29 and the concomitant activation of its targets are restricted to the initial acute phase following injury. We examined the cortical transcriptome at additional reperfusion time points (6, 12, 24hrs) to generate a time-course RNA profile of both miRNA and mRNAs. Time-dependent miRNAseq revealed that the loss of miR-29 persists and is enhanced through 24hrs following injury. This expression pattern was consistent among all three miR-29 family members, while another equally abundant brain miRNA, let-7a, equally abundant to miR-29a, showed no significant changes (Figure 4B). Time-course mRNA profiling illustrated activation of canonical factors, ie. heat shock proteins and inflammatory cytokines, across all time points (Figure S4A-B, Supplementary Table 4). Interestingly, while mRNA profiling at 3hrs showed no changes in the abundance of miR-29 target transcripts (Figure 3A), we observed accumulations of miR-29 target mRNA levels at reperfusion time-points of 6, 12, and 24hrs (Figure 4C-E). Transcript accumulation correlated with increasing time after I/R, reflecting the precipitous loss of miR-29 over time (Figure 4B). This expression pattern was seen exclusively in the RNAseq fold change distribution of miR-29 targets and not of control miRNA targets (let-7, top 10 brain miRNA). Taken together, the observations from this time-course expression profile, combined with the CLIP and RPF results, illustrate the dynamic mechanism of miRNA associated post-transcriptional gene regulation in brain injury response: the dramatic and persistent down-regulation of miR-29 following stroke initiates a temporally distinct cascade of target activation, exclusively by translational up-regulation at first followed by a steady increase in mRNA levels.

Loss of miR-29 is required for activation of its targets

To determine whether the miR-29 loss directly activate miR-29 target transcripts, we turned to an established *in vitro* model system for cerebral ischemic injury. Cultured mouse cortical cells (consisting of ~70% cortical neurons, ~30% astrocytes, and a few microglia cells) were exposed to oxygen-glucose deprivation (OGD). After OGD, the cultures were replenished with full growth media and re-oxygenated to simulate reperfusion (Tasca et al., 2014). This culture system allows for direct quantification of gene expression and is readily accessible to manipulation of cellular miRNA levels for functional testing. Using this approach, we observed miR-29 loss after OGD exposure, as measured by independent qPCR of family members, -

29a, -29b, and -29c (Figure 5A). Global activation of miR-29 targets was also readily observed, as CDF plots of RNAseq fold change distributions (OGD vs control) show a collective increase of miR-29 targets relative to global transcriptome-and to non-targets (Figure 5B).

Multiple studies reveal miRNA target recognition can include interactions beyond traditional seed matched pairing (Grimson et al., 2007, Lal et al., 2009, Loeb et al., 2012, Chi et al., 2012, Helwak et al., 2013, Moore et al., 2015). We examined miR-29 target activation as a function of target discovery using informatically predicted canonical sites (TargetScan, 7-8mer seed matched, highly conserved), or by an unbiased assessment of empirically defined sites (CLEAR-CLIP, include both canonical and non-canonical interactions). Activated targets were more enriched in empirically defined sites compared to targets exclusively defined by TargetScan (Figure 5C). While we observed significant changes in all 3'UTR seed types bound by miR-29, the largest increase was among sites with 7-8mer seeds and, unexpectedly, among those with non-canonical seed sites (Figure 5D). These observations indicate significant roles mediated by non-canonical miR-29 targeting in ischemic brain injury. In summary, brain CLEAR-CLIP data proved an important resource to elucidate miRNA targets in studying the role of miRNAs following ischemia.

To address the requirement of miR-29 loss in activating downstream targets in ischemia, we used a lenti-viral gene delivery approach to rescue the miRNA impairment in OGD-induced cultures. Quantitative PCR for miR-29 in OGD cortical cultures showed effective restoration of mature miRNA levels with infection by miR-29 encoding lenti-virus but not by empty virus control (Figure 5E). Accordingly, RNAseq analysis revealed that this restoration was sufficient to suppress the global miR-29 target activation to below baseline levels in the presence of OGD (Figure 5F). These data establishes the loss of miR-29 in I/R injury as a necessary event for the global activation its targets, and that its corresponding impact on the transcriptome is rescued by restoring miR-29.

miR-29 down-regulation activates a gene network governing brain homeostasis and neuro-protection.

In order to gain insight into the physiological roles played by activated miR-29 targets in I/R injury response, we performed pathway enrichment analysis of CLIP identified miR-29 targets (Figure 6A). The top pathways included fundamental stress responses to deficits of oxygen and ATP synthesis, such as hypoxia inducible factor (HIF1α) signaling, eNOS signaling, and p53 signaling. In addition, cytokine and growth factor signaling by Interleukin (ILK) and VEGF, along with corresponding intracellular effectors, CREB and PI3K/Akt, were enriched. The most significantly enriched pathway was glutamate receptor-signaling, in response to excitotoxicity, a primary cause of tissue damage elicited by ischemia and reperfusion stress (Iadecola and Anrather, 2011). Genes under miR-29 control in this pathway included glial enriched glutamate transporter, *Slc1a2* (GLT-1), as well as synonymous glutamate receptors *Gria3* (Glur3) and *Grm3* (mGluR3).

We directly tested miR-29's ability to influence extracellular glutamate levels in *in vitro* stroke. Over-expression of miR-29 by lentivirus exacerbated OGD-dependent increase in extracellular glutamate concentrations, relative to control expression of an empty virus (Figure 5E, 6B). Taken together, these results indicate that dysregulation of miR-29 plays a fundamental role in counteracting ischemic damage by dampening toxic glutamate levels.

In the brain, miR-29 is predominantly expressed by astrocytes, with moderate levels detected in neurons (Smirnova et al., 2005), suggesting that a major role for miR-29 in regulating astrocyte physiology. Therefore, we examined miR-29 targets whose expression is also

restricted to astrocytes. We ranked our down-regulated AGO peaks by their relative enrichment in astrocytes, using a published reference for brain cell-type transcriptomes (Zhang et al., 2014) (Figure 6D). The top astroctytic miR-29 direct targets included transcripts encoding key players of ischemic responses established by our GO analysis (Figure 6A), *Grm3*, *Slc1a2*, and *Vegfa*, glutamate signaling and HIF1α responders. The most significant gene aquaporin 4 (*Aqp4*), is enriched in astrocytic end-feet abutting cerebral microvessels and plays a key role in water balance, edema, blood brain barrier permeability and subsequent neuroinflammation in stroke (Fukuda and Badaut, 2012), and has been suggested to be a target of miRNA control (Sepramaniam et al., 2010; Wang et al., 2015). The discovery of a known response factor, *Aqp4,* by AGO CLIP, supports our strategy to define miRNA regulatory networks relevant to stroke physiology.

We directly examined the regulation and expression of these top miR-29 regulated genes in stroke, including the key players of glutamate signaling (*Grm3, Slc1a2, Gria3*), known hypoxia and ischemic stroke responders (*Vegfa, Aqp4),* in addition to downstream effectors of activated signaling (*Akt3, Gsk3b*). We observed decreases among AGO peaks at corresponding miR-29 sites within conserved and non-conserved regions (Figure 6C, S5B). Moreover, quantitative expression analysis of protein levels demonstrated elevated expression in stroke brain (Figure 6E), with varying kinetics in steady-state protein levels over reperfusion time (Figure S5A). Importantly, the activation of 6 of these 7 targets was rescued by miR-29 lenti-viral expression, reverting their RNA levels to near baseline in OGD modeled ischemic conditions (Figure 6F, S5C). Taken together, the data reveal a master regulatory network exists to restore essential brain homeostatic functions activated by a loss of miR-29 family of miRNAs in stroke.

Identification of human genetic polymorphisms in stroke-associated miR-29 sites

To apply our findings from model systems to human stroke, we intersected our differential CLIP sites identified in mouse I/R injured brain with human brain AGO CLIP data to look for orthologous, stroke-associated, miRNA regulatory events in human brain. We generated AGO CLIP data using post-mortem medial prefrontal cortex tissues from 6 individuals, and, to increase biological complexity for robust peak calling, merged our data with an existing human AGO CLIP resource (Boudreau et al., 2014), generated from motor cortex and cingulate gyrus of 17 individuals. Together, these data defined 23,662 reproducible (peak height >50) human AGO brain peaks. 999 mouse stroke peaks (out of 1,190, Figure 1D) re-mapped to orthologous human sites, out of which 429 sites intersected with human AGO CLIP peaks (Figure 7A), representing a cohort of stroke-associated human miRNA regulatory sites. Evaluation of these peaks for miRNA binding motifs revealed enrichment of target sites for multiple human brain miRNAs, including miR-29 and another stroke and hypoxia associated miRNA, miR-181 (Figure 7B) (Ouyang et al., 2012, Zhang et al., 2012), providing an important resource to further our understanding of miRNA regulation in complex brain disease.

The human genome contains thousands of variants that can potentially alter miRNA binding. Allele specific polymorphisms in miRNA binding sites have been shown to vary miRNA function and play essential roles in complex human diseases, including cancer, diabetes, and Alzheimer's diseases (Brewster et al., 2012, Zhao et al., 2013, Delay et al., 2011). We implemented an informatic analysis to identify single nucleotide polymorphisms within the 429 stoke-associated miRNA target sites. We relied on existing SNPs previously submitted to NCBI's dbSNP resource and intersected them with 7-8mer seed containing, miRNA binding sites within our 429 cohort. We identified 332 unique single nucleotide variations among 165 miRNA binding sites representing 222 miRNAs across 117 genes (Supplementary Table 5).

Notably, we identified 6 SNPs that modify miR-29 target sequences. The alternative alleles among these 6 sites represent both rare and common variants within the human population. 5 out of the 6 variants have the potential to disrupt miR-29 binding, while 1 may enhance miR-29 seed pairing (Figure 7C, S6). Some SNPs fell within a single 3'UTR, such as rs147077348 and rs574793836, polymorphisms for two distinct miR-29 binding sites in *SPARC*, and rs191276899 and rs757907139, altering distinct nucleotides within a single miR-29 seed binding sequence of *WASF1* 3'UTR. Interestingly, we identified a SNP within a validated stroke target, *AQP4*, rs760955838. This rare G>A variant (rs760955838), with a higher predicted binding energy coefficient, has the potential to markedly weaken miR-29 seed pairing and affect *AQP4* gene expression (Figure 7D). These observations illustrate a strategy to reveal human stroke-associated miRNAs and their target site variations that may be associated with clinical stroke outcome. The datasets utilized in this study thus provide a rich resource and approach to investigating disease relevant polymorphisms altering miRNA functions.

DISCUSSION

Empirical investigation of unique biological and pathological states is imperative for elucidating mechanisms underlying relevant physiology. AGO-HITS CLIP affords the power to systemically identify, quantify and compare miRNA:target interactions in normal and disease brain, prevailing informatic predictions. Strictly informatic strategies currently use data made from pooled, often irrelevant tissue types, and rely on evolutionary constraints for interpretation. Several reports using this strategy have found primary effects of miRNA perturbations impact mRNA levels (Guo et al., 2010; Eichhorn et al., 2014). In this study, AGO-CLIP allowed us to find that down regulation of miR-29 in the brain after I/R leads to an acute, strong translational effect with minimal impact on mRNA levels. Such divergent miRNA actions, limited to distinct physiological circumstances, have been previously described, as in the observation that translational effects precede mRNA turnover in exerting miR-430 control during early phases of zebrafish development (Bazzini et al., 2012). Additionally, reminiscent of molecular responses seen underlying axonal regeneration and repair upon neuronal injury (Jung et al., 2012; Rishal and Fainzilber, 2013), the immediate translational activation of miR-29 targets maybe the most pertinent response to modulate the acute and rapid cellular responses required for counteracting ischemic insult (Iadecola and Anrather, 2011).

Unexpectedly, AGO-CLIP, interpreted together with brain CLEAR-CLIP data, revealed that non-canonical seed pairing events contributed to many functional miR-29 targeting events. Auxiliary target interactions at miRNA's 3' ends give distinction among miRNA family members with shared seeds (Brennecke et al., 2005; Moore et al., 2015, Broughton et al., 2016), and could compensate imperfect seed pairing for miRNAs with AU-rich seed motifs (Moore et al., 2015). Although miR-29 seed sequence is not AU-rich, further characterization of compensatory pairings among identified seedless interactions may yield mechanistic insights distinct from canonical miRNA targeting, and help delineate gene 'sub-networks' playing disparate roles in I/R brain injury.

Altered miR-29 levels in animal models of stroke have been previously reported, however, with varying conclusions depending on the experimental model and brain region being examined (Yuan et al., 2010, Ouyang et al., 2013), with limited follow-up studies on global molecular consequences. Discrepancies may be attributed to brain region-specific regulation of miR-29 levels, or to distinct miR-29 target transcriptomes present in different regions. Although *not* identified in this study, the proposed molecular events causing loss of miR-29 include ischemia activated 12-lipoxygenase (Khanna et al., 2013), and suppression by transcriptional repressor,

REST, activated by global ischemia. Over-expression of individual miR-29 family members has shown to improve stroke outcome in animal models by reducing infarct volume (Pandi et al., 2013, Wang et al., 2015, Khanna et al., 2013), and enhance post-stroke sensorimotor function (Khanna et al., 2013). The proposed mechanism of neuroprotection for each of these studies differ, and include the activation of DNA methyltransferase, DNMT3a, upon miR-29c loss (Pandi et al., 2013) and attenuating blood brain barrier disruption and subsequent vasogenic edema formation through relieving miR-29b repression of AQP4 (Wang et al., 2015). These studies, however insightful, by isolating a single miRNA:target interaction and considering an individual miR-29 family member at a time, covey a limited perspective of the gross systems-wide response.

We uncovered a novel regulatory network of direct miR-29 targets that together counteract the deleterious effects of glutamate excitotoxicity. The accumulation of extracellular glutamate is a cardinal event contributing to cell death and pathology after ischemia (Benveniste et al., 1984, Choi and Rothman, 1990, Moskowitz et al., 2011). Excitatory amino acid transporters (EAATs) play a paramount role in maintaining homeostatic levels of glutamate by its rapid uptake from extracellular space. We find that GLT-1 (EAAT2), a major glutamate transporter in the brain, responsible for more than 90% of total glutamate uptake (Maragakis et al., 2004) is a miR-29 target. Studies modifying GLT-1 gene expression levels in stroke indicate a protective role of over-expression in animals, associated with reduced levels of extra-cellular glutamate (Harvey et al., 2011). mGluR3, another direct miR-29 target identified in this study, is a member of group-II metabotropic glutamate receptors, activated by glutamate neurotransmitter and enriched in adult astrocytes (Sun et al., 2013). mGluR agonists show potent neuroprotective activity in both *in vitro* and animal models of ischemic injury (Flor et al., 2002). Though mechanisms of how mGluR agonists exert neuroprotection remain unclear, it is enhanced by the presence of glial cells (Kingston et al., 1999), suggesting a direct role of astrocytic mGluR3. Direct targeting of miRNA regulatory sites of glutamate signaling effectors identified in this study may be a precise and feasible therapeutic approach to modulate their expression levels and mitigate accumulation of toxic glutamate concentrations in I/R brain injury.

Stroke-relevant miR-29 target sites identified with AGO CLIP not only revealed thousands of targets important for underlying mechanism of I/R brain injury, but provide a powerful reference for determining genomic variants likely associated with disease. Interestingly, loss of miR-29 has also been observed in more archetypal neurodegenerative diseases, such as Alzheimer's and Huntington's brains, *in vitro* model of spinocerebellar ataxia 17, and in sciatic nerve injury response (Hébert et al., 2008, Shioya et al., 2010, Johnson et al., 2008, Roshan et al., 2012, Verrier, et al., 2009), suggesting an expansive and crucial role for miR-29 in brain homeostasis. A comprehensive, unbiased characterization of miR-29 targets in these pathological states, integrated with our findings in stroke, will provide powerful insights into both common and distinct pathological gene networks, help elucidate universal miR-29 target site variants associated with risk or outcome across multiple neurodegenerative diseases, and allow elegant designs for therapeutics of broad benefit.

FIGURES

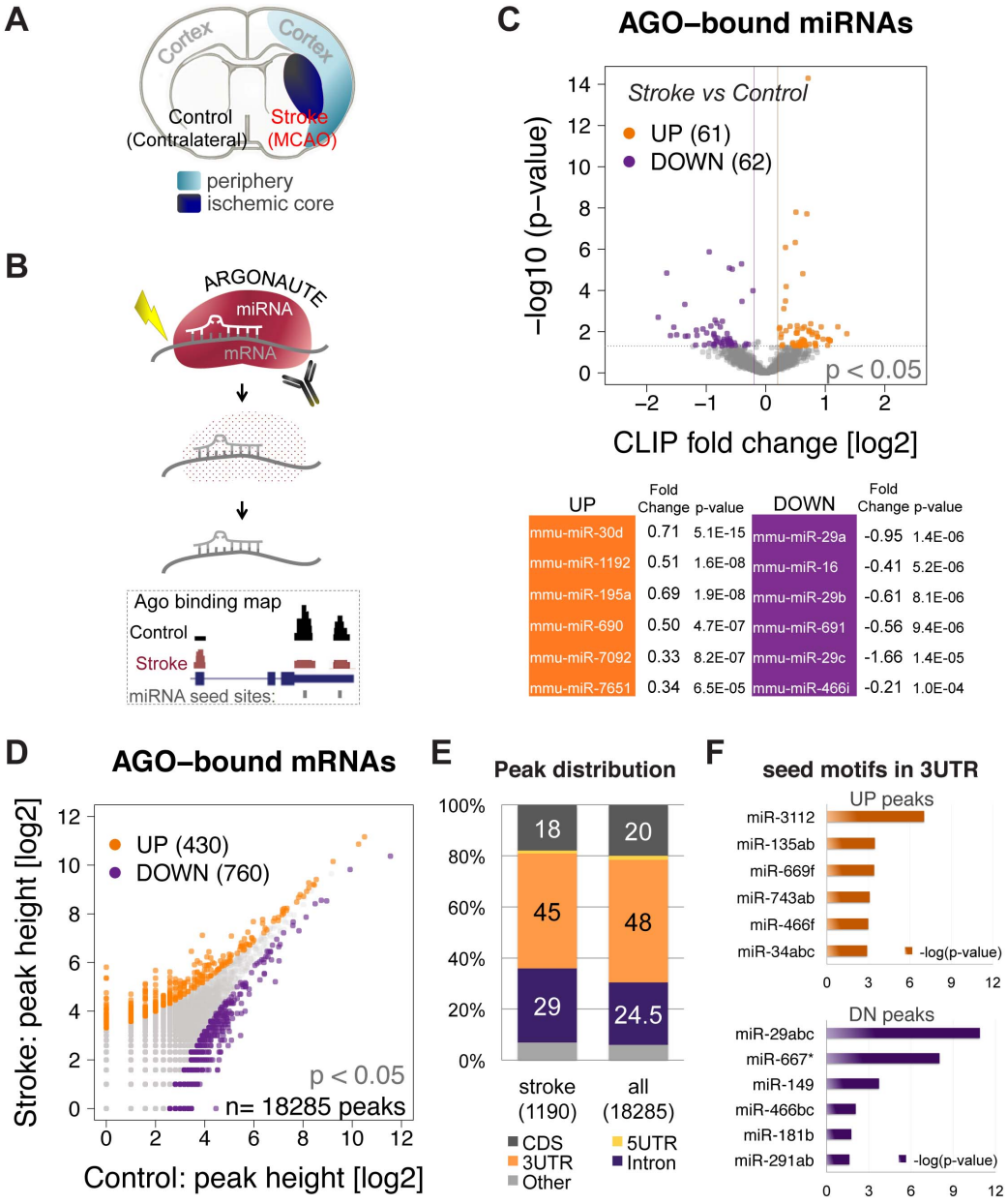

Figure 1. Identification of stroke-associated AGO:RNA interactions using CLIP. (A) Mouse brain coronal slice illustrating MCAO model. The contralateral hemisphere analyzed as 'Control,' while MCAO performed hemisphere analyzed as 'Stroke.' Cortical 'periphery' (light blue) is distinguished from 'ischemic core' (dark blue) within the ischemic territory. (B) Stroke AGO HITS-CLIP schema. 1) UV-crosslink brain AGO to interacting RNAs, 2) IP and purify AGO:RNA complexes, 3) proteinase digest AGO for isolation of RNA tags, 4) library generation and hi-throughput sequencing, 5) mapping to reference genome and difference analysis. (C) Volcano plot depicting AGO-bound miRNAs increasing (orange) or decreasing (purple) in stroke condition. The two vertical lines indicate log2 fold change cut-off, >|0.2|, the horizontal dotted line indicates p-value cut-off, p<0.05, determined by binomial testing. Table lists top 6 miRNAs differentially bound by AGO in stroke, ranked by p-values. (D) Scatter plot of peak height intensities of 18,285 AGO-bound mRNA peaks found in either control or stroke. Difference analysis used to determine increased (orange) and decreased (purple) binding peaks using a p-value cut-off of p<0.05. (E) Distribution of peaks among annotated genomic regions, for peaks changed in stroke and for all identified peaks. (F) Motif enrichment analysis of 3'UTR peaks, increased (top) or decreased (bottom) in stroke. All stroke samples collected after 3hr reperfusion following MCAO. See also Figure S1.

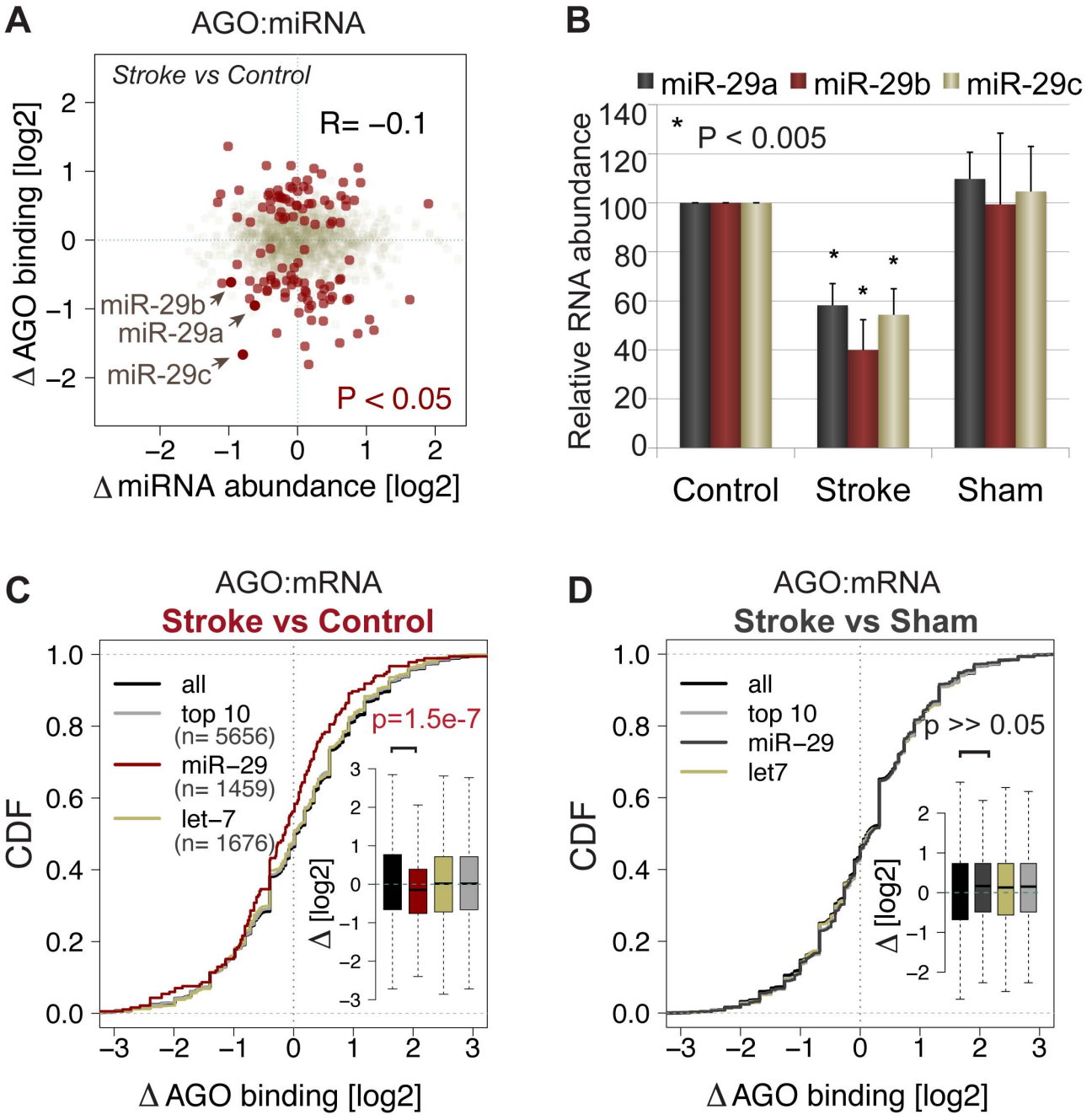

Figure 2. A global loss of miR-29 regulation upon acute I/R insult. (A) Scatter plot of log2 fold change in miRNA abundance (x-axis: miRNAseq) *vs*. differences in AGO-binding (y-axis: CLIP). Dark red dots indicate miRNAs that met p-value cut-off of p<0.05, binomial testing, for both assays. Arrows highlight miR-29 family members, -29a, -29b, -29c. R indicate Pearson's correlation coefficient. (B) Quantitative PCR show abundance of miR-29a, -29b, and -29c miRNAs in control, stoke or sham cortical tissues normalized to levels in control. P-values generated using Student's t test. Error bars represent ±SD. Cumulative density function (CDF) plot of AGO-bound mRNA (CLIP) log2 fold changes in (C) stroke, or in (D) sham. Curves represent collective CLIP peak height changes among miR-29, let-7 or top 10 brain miRNA target sites. Same distribution plotted as box plot (insets), and depicts distribution mean fold changes (black notches). P-values calculated using Mann-Whitney-Wilcoxon test, miR-29 distribution to all. All stroke samples collected after 3hr reperfusion following MCAO. See also Figure S2.

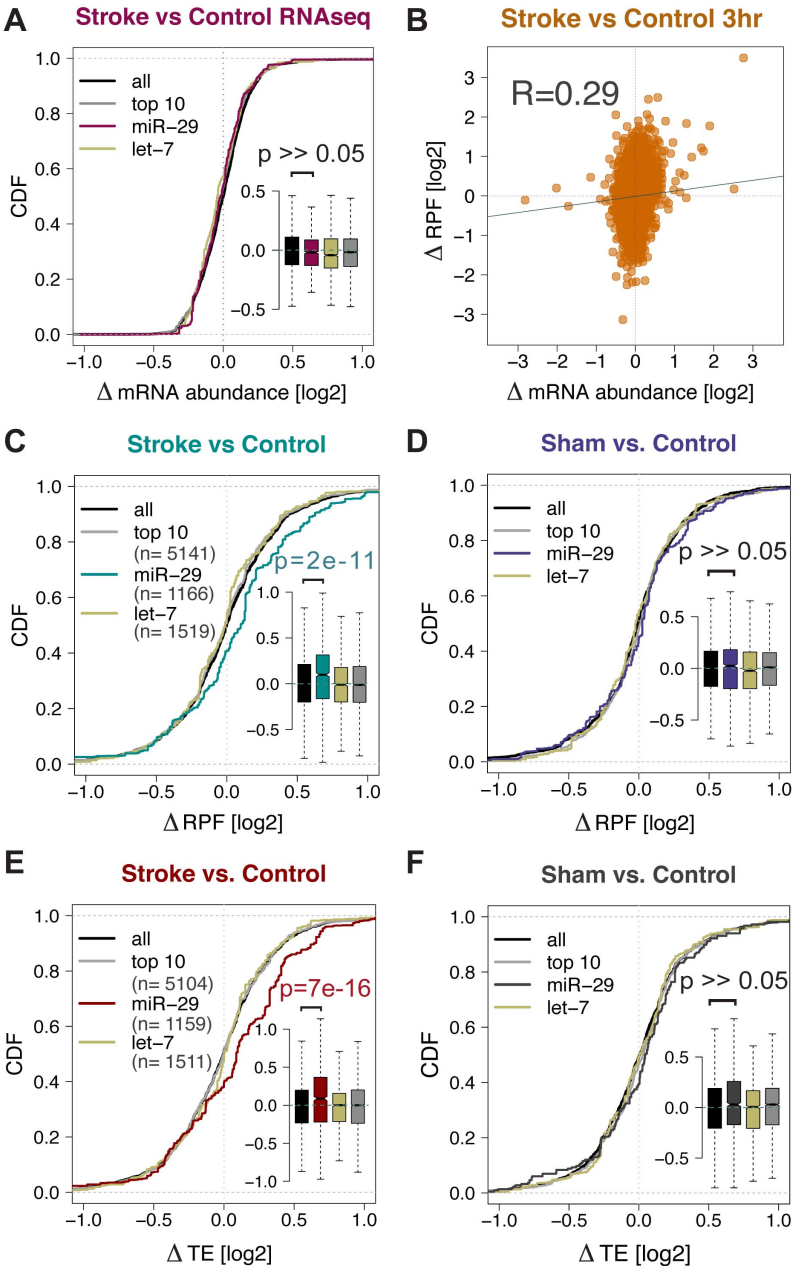

Figure 3. Functional consequences of miR-29 down regulation at an early time point after injury. (A) CDF plot illustrate distributions of mRNA abundance changes in stroke assayed by RNAseq. Curves represent collective log2 fold changes among genes with miR-29, let-7, or top10 brain target sites. Distributive plot also plotted as box plots (inset), and depicts distribution mean fold changes (black notches). P-value calculated using Mann-Whitney-Wilcoxon test comparing miR-29 subset distribution to all genes. (B) Stroke log2 fold change RNA abundance (ΔRNAseq) plotted against log2 fold change ribosomal association (ΔRPF), R indicate Pearson's correlation coefficient. Diagonal line denotes linear regression. (C-F) CDF as in (A) plotting changes assayed by RPF in (C) stroke, or (D) in sham, and TE calculation for (E) stroke, (F) sham. All stroke samples collected after 3hr reperfusion following MCAO. See also Figure S3.

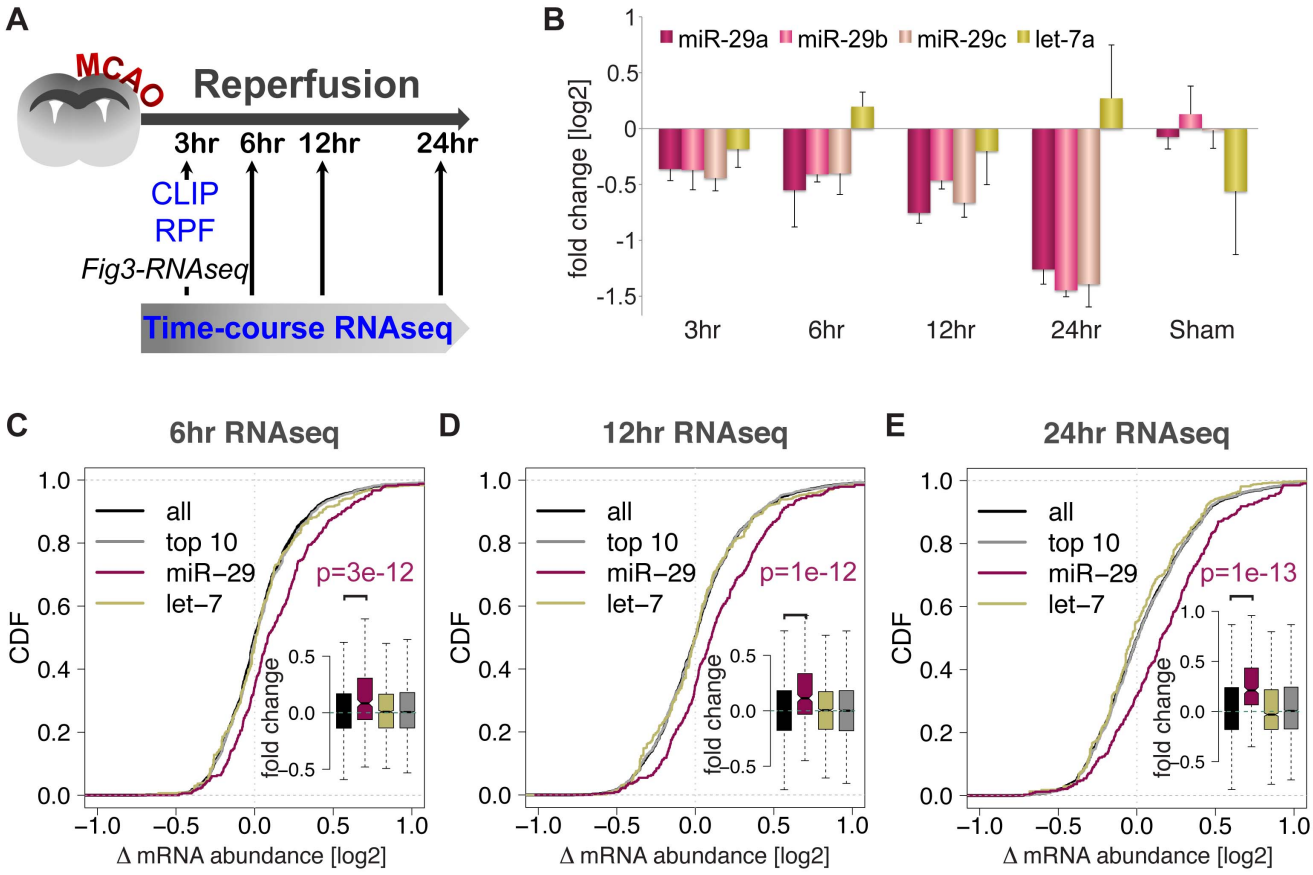

Figure 4. Time-course expression profiling following stroke. (A) RNAseq time-course experiment used samples collected at defined time points after MCAO and reperfusion. Time-course data relative to AGO-CLIP, RPF, Fig3 RNAseq data generated using 3hr reperfusion time point. (B) Log2 fold changes, relative to control, of miR-29a, -29b, -29c, and let-7a abundance at 3, 6, 12, and 24hr reperfusion time points, assayed by miRNAseq. Error bars represent ±SD. (C-D) CDF plots show distributions of mRNAseq fold changes in stroke time points of 6hr, 12hr, and 24hrs. Curves represent collective changes among genes with miR-29, let-7, or top10 brain miRNA target binding sites. Inset box plots indicate distribution mean fold changes by black notches, p-values generated using Mann-Whitney-Wilcoxon test, miR-29 distribution to all. See also Figure S4.

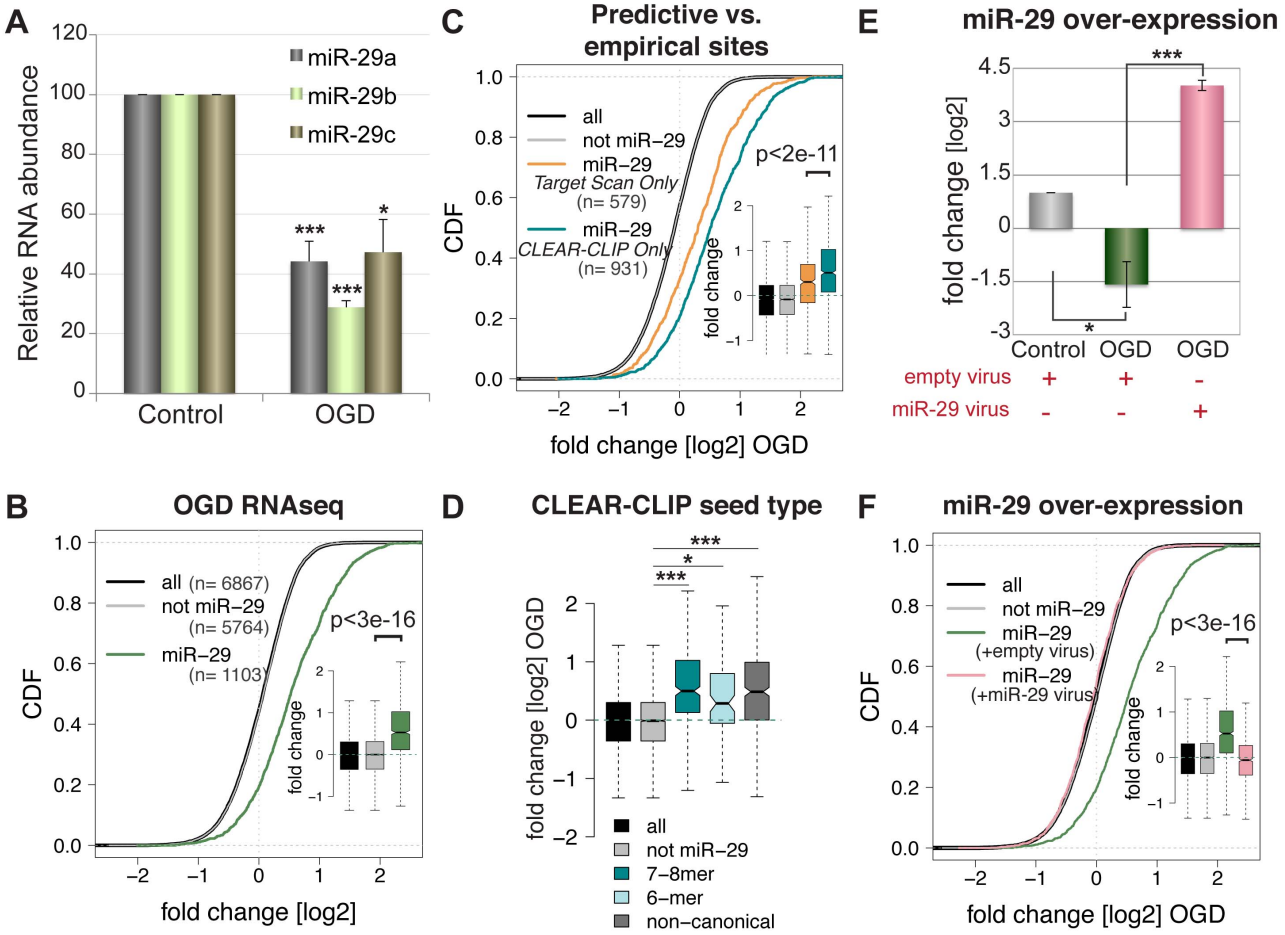

Figure 5. miR-29 loss in oxygen-glucose deprivation model of stroke. (A) Quantitative PCR measured miR-29a, -29b, -29c mature miRNA levels in OGD treated cortical cultures relative to untreated control. *P<0.005, ***P<5e-6, Student's t test. CDFs of OGD vs. control RNAseq fold changes for distributive curves of (B) miR-29 targets to others, or 'not miR-29,' (C) miR-29 targets exclusively predicted by TargetScan to those empirically defined by CLEAR-CLIP, inset box plots depict distribution mean fold changes (black notches). (D) Box plot illustrates OGD RNAseq fold change distributions of miR-29 target subgroups defined by seed types to all other targets, black notches indicate means. *P<1.7e-11, ***P<2.2e-16. (E) Quantitative PCR show relative expression fold changes of miR-29 in OGD conditions infected with indicated lenti-virus normalized to control. *P<0.05, ***P<0.005, Student's t test. (F) CDF plot of OGD RNAseq fold change distributions of miR-29 targets infected with empty or with miR-29 virus. P-values for all distributive data calculated using Mann-Whitney-Wilcoxon test. All error bars represent ±SD.

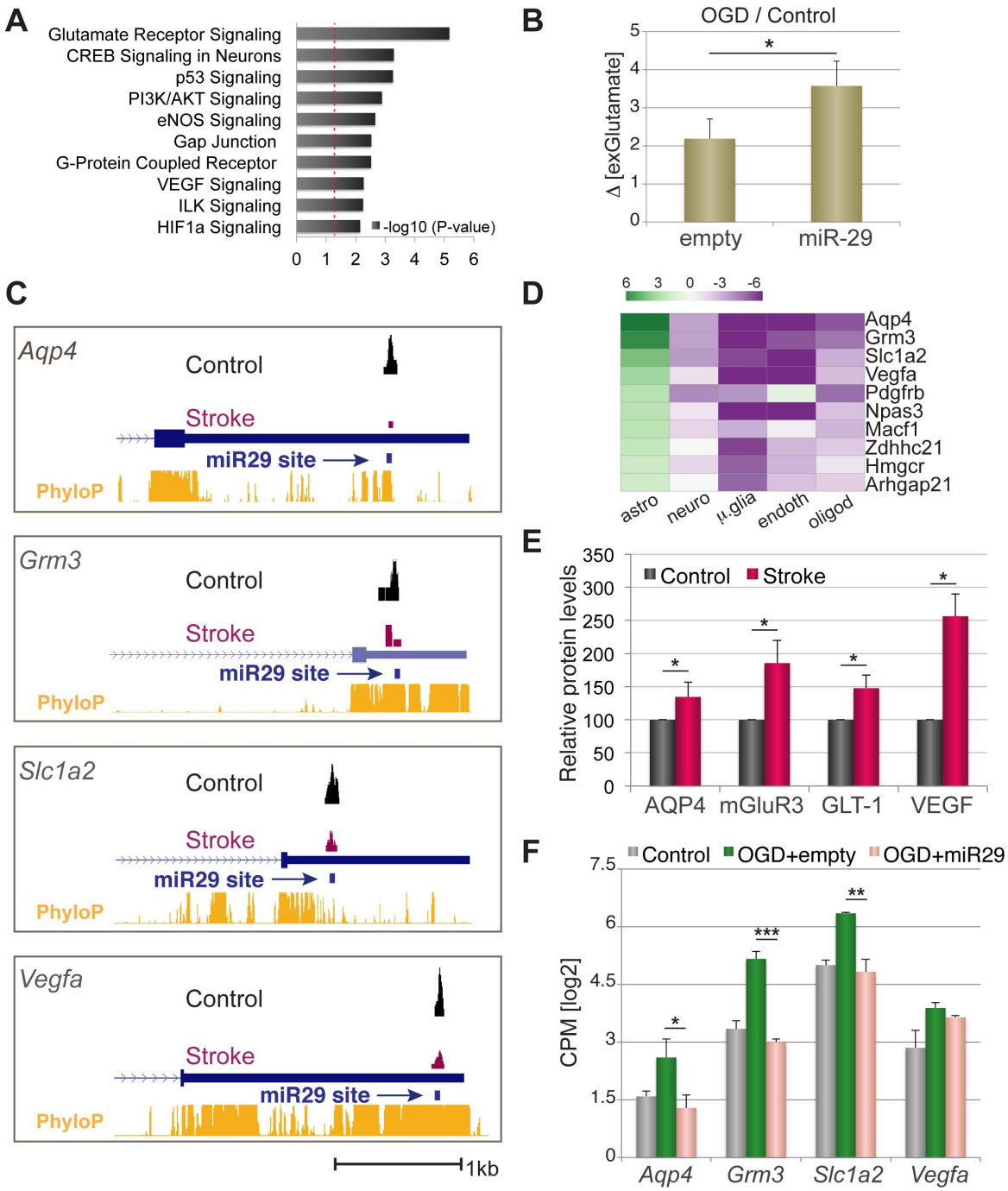

Figure 6. Activation of miR-29 regulated neuroprotective factors (A) Pathway analysis of miR-29 targets containing 3'UTR AGO CLIP peaks that decrease in stroke, dotted red line indicates p=0.05. (B) Quantification of extracellular glutamate levels after OGD. Fold change(Δ) in glutamate concentrations calculated between OGD vs Control in miR-29 or empty lenti-virus infected samples. (C) Genome Browser views of 3'UTRs for top four astrocyte-enriched miR-29 targets (*Aqp4*, *Grm3*, *Scl1a2*, and *Vegfa*). Arrow points to respective CLEAR-CLIP defined miR29 binding sites, control (black peaks) and stroke (magenta peaks). Yellow track indicate PhyloP scores for corresponding gene regions. (D) miR-29 targets from (A) ranked by their astrocyte log2 enrichment values, top 10 genes plotted as heatmap. (E) Quantitative westerns depict relative protein levels for each gene normalized to levels in sham control, total protein collected from cortical tissues of sham or MCAO animals following 3hr reperfusion. (F) Normalized [log2] CPM values calculated using RNAseq in cortical cultures of untreated control, OGD treated and infected with empty or miR-29 over-expression lenti-virus. *P<0.05, **P<0.005, ***P<5E-4, Student's t test. All error bars represent ±SD. See also Figure S5.

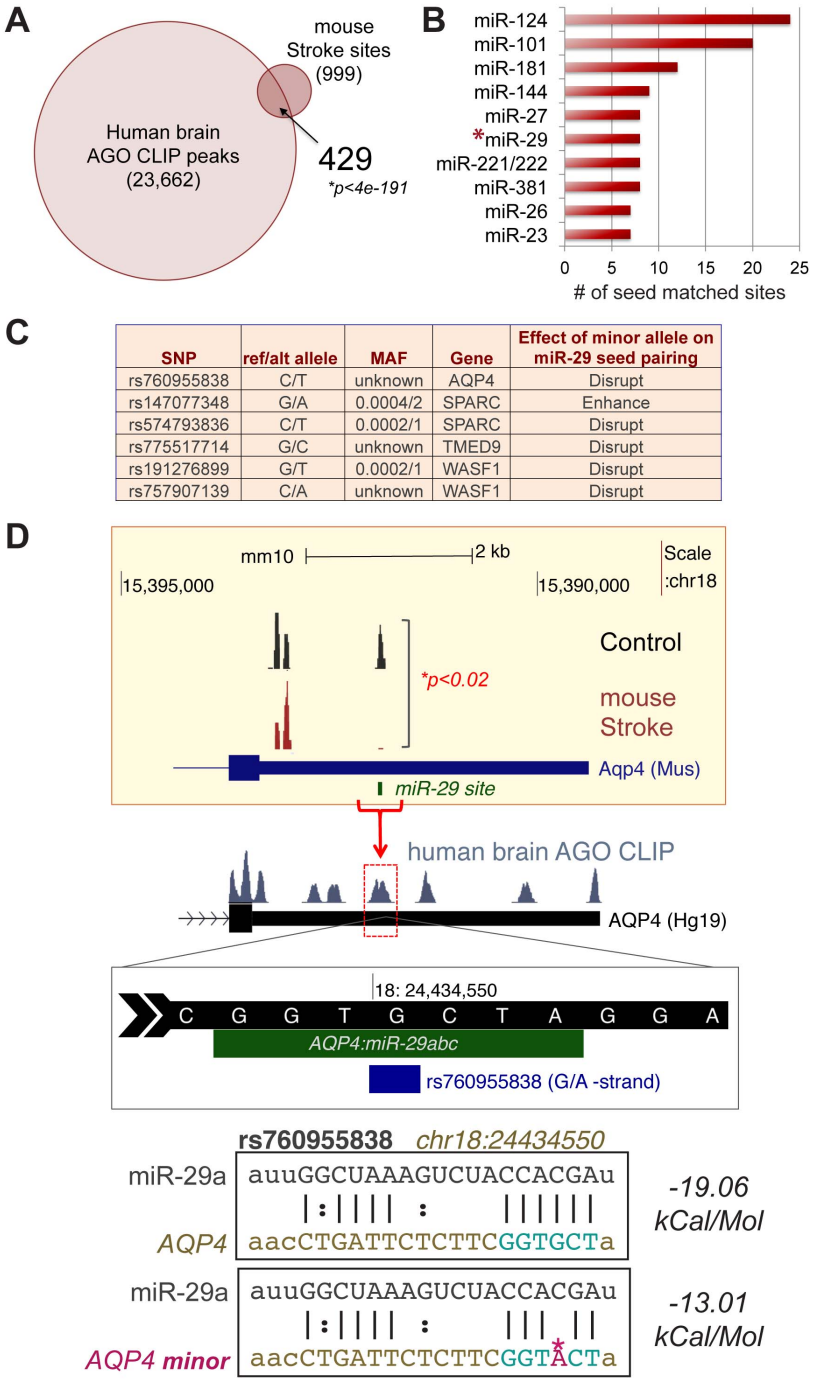

SNP	ref/alt allele	MAF	Gene	Effect of minor allele on miR-29 seed pairing
rs760955838	C/T	unknown	AQP4	Disrupt
rs147077348	G/A	0.0004/2	SPARC	Enhance
rs574793836	C/T	0.0002/1	SPARC	Disrupt
rs775517714	G/C	unknown	TMED9	Disrupt
rs191276899	G/T	0.0002/1	WASF1	Disrupt
rs757907139	C/A	unknown	WASF1	Disrupt

Figure 7. Stroke-associated miR-29 target site polymorphisms (A) Venn diagram depicting overlap of human brain AGO CLIP peak regions with, mouse stroke identified sites, conserved across two species. *Hypergeometric test was used to calculate p-value. (B) Bar chart of top 10 miRNA seed matched sites among 429 stroke-associated AGO targets in human brain. Asterisk highlights miR-29. (C) Table of 6 identified SNPs in stroke-associated miR-29 target sites, reference vs. alternative allele, minor allele frequency (MAF), if known, associated gene, genomic location, and predicted influence on seed pairing. (D) Genome browser views of Aquaporin 4 3'UTRs, mm10 (top), hg19 (below). Differential AGO CLIP peak in stroke bracketed, *t-test calculated p-value. Red arrowed bracket points to homologous site in human genome (second browser view), corresponding AGO peak denoted by red dotted square. The sequence at this peak position shown is below highlighting the miR-29 target site (green) and SNP, rs760955838 (dark blue). Bottom diagram depict differences in miR-29a pairing to AQP4 target site in for rs70955838 reference allele (top panel), and minor allele (bottom panel). Computationally predicted binding energy coefficients indicated. Minor allele in seed sequence marked with pink, asterisk. See also Figure S6.

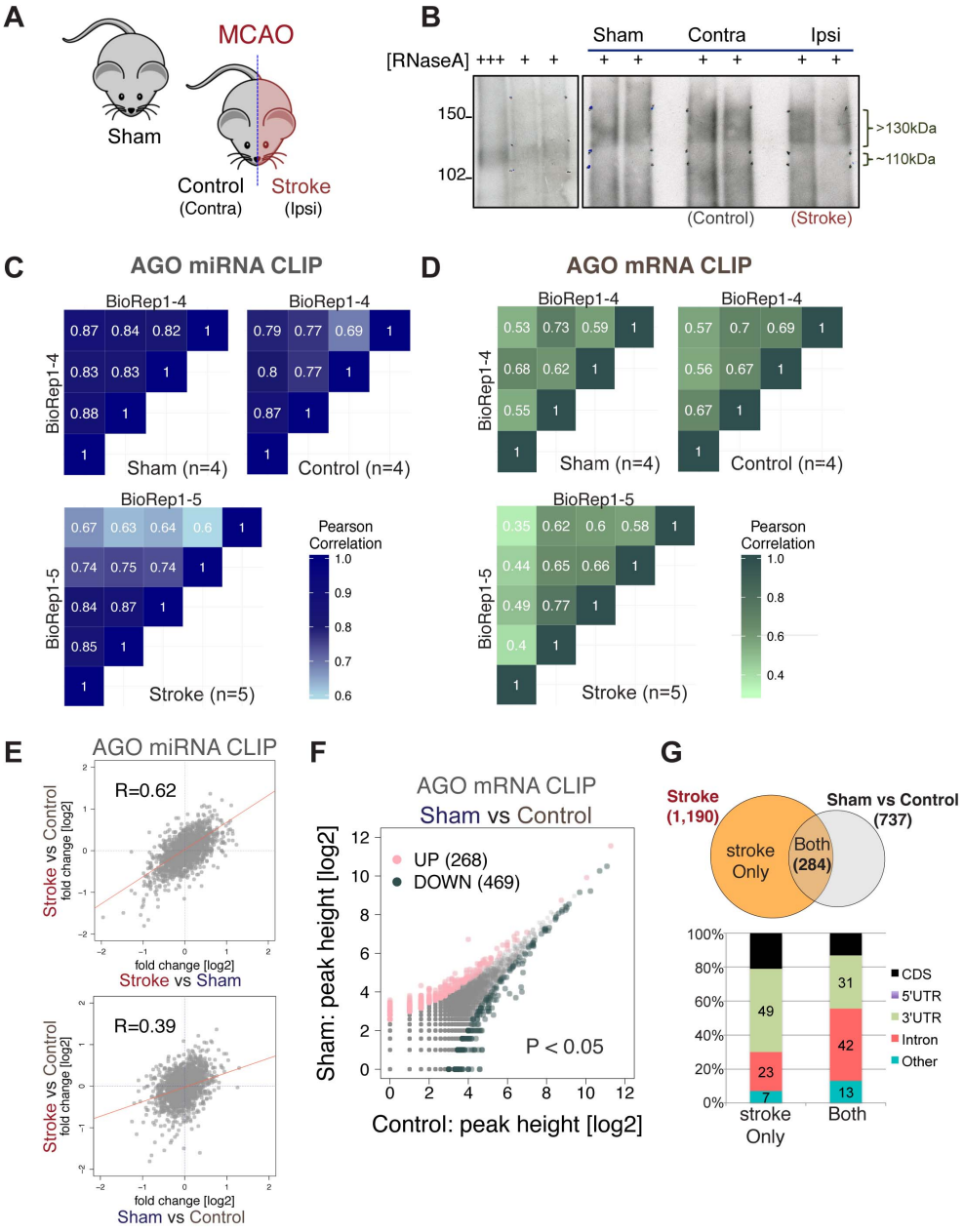

Supplementary Figure 1. Stroke AGO-CLIP miRNA and mRNAs, related to Figure 1. (A) Mouse MCAO stroke model. MCAO performed on the ipsilateral (left) cerebral hemisphere, contralateral (right) is analyzed as control. Sham surgery animal serves as secondary control. (B) Autoradiogram of ^{32}P-labeled RNA crosslinked to AGO. IP purified AGO from untreated (left 3 lanes), sham, control, or stroke treated cortical tissue ran on SDS-PAGE. High [+++] RNaseA or complete digestion, low [+] RNaseA or partcial digestion of AGO-RNA complexes. Right brackets indicate complexes isolated for subsequent cloning and high-throughput sequencing analysis. Correlation heatmaps of biological replicates for (C) AGO miRNA CLIP tags and (D) AGO mRNA CLIP tags in peaks. Correlations across 4 replicates for sham, 4 replicates for control, and 5 replicates for stroke are shown. (E) Scatter plots of log2 fold changes of AGO bound miRNAs demonstrating correlation between changes in stroke compared to either controls (top), or change in stroke compared to change in sham (bottom). Red diagonal lines denote linear regression. (F) Scatter plot depicts peak height intensities of AGO-bound mRNA peaks in either control or sham conditions. Difference analysis used to determine increased (light pink) and decreased (forest green) binding peaks using a p-value cut-off of $p<0.05$, binomial testing. (G) Venn diagram show overlap of stroke peaks to sham peaks. Distribution bar plot of peaks among annotated genomic regions, changing in stroke only, or in both stroke & sham. All stroke samples collected after 3hr reperfusion following MCAO. All R-values indicate Pearson's correlation coefficient.

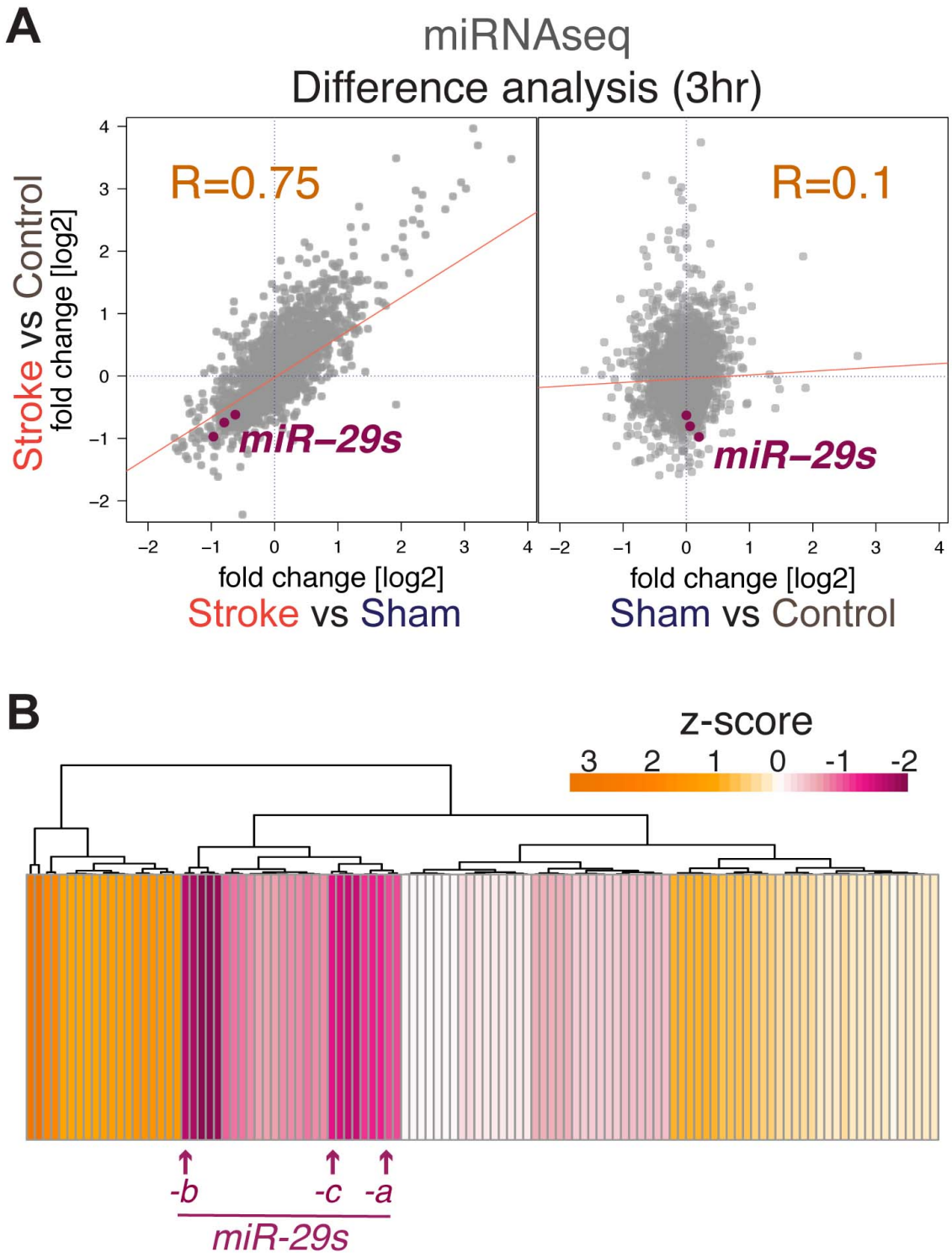

Supplementary Figure 2. miRNAseq in stroke, related to Figure 2. (A) Scatter plots of miRNAseq log2 fold changes in stroke demonstrating correlation between stroke compared to either controls (left), or change in stroke compared to change in sham, miR-29 data points highlighted in dark pink. R indicate Pearson's correlation coefficient. Red diagonal lines denote linear regression. (B) Hierarchical clustering and heatmap visualization of differentially expressed miRNAs in stroke. Z-scores calculated using miRNAseq log2 fold change in stroke for miRNAs identified by AGO-CLIP. Orange is up-regulated, while pink is down-regulated miRNAs. Arrows point toward miR-29 family members within a cluster of up-regulated miRNAs.

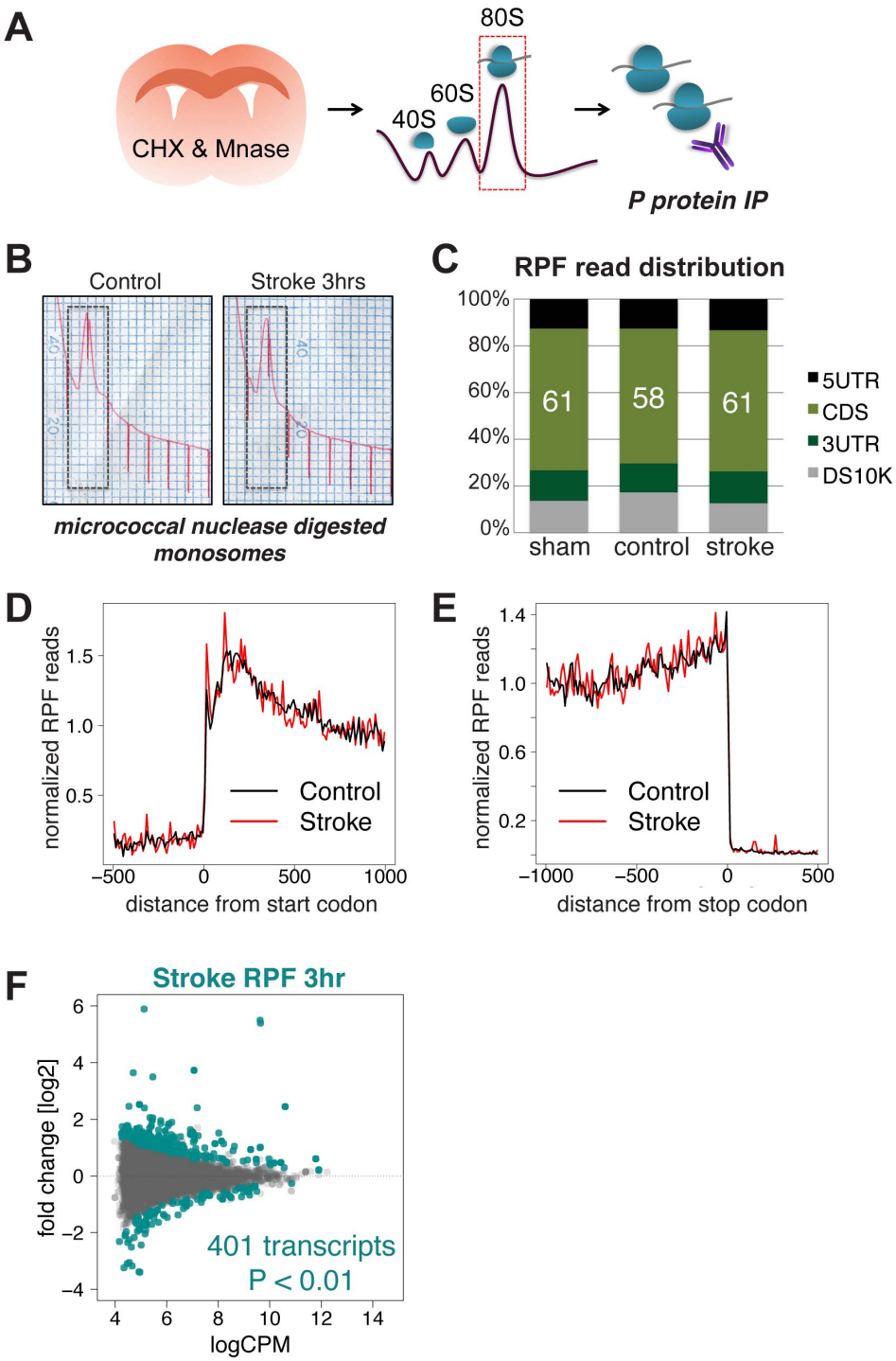

Supplementary Figure 3. Stroke brain ribosomal profiling, related to Figure 3. (A) **RPF schema.** CHX Cycloheximide (CHX), micrococcal nuclease (Mnase), P0, P1, P2 large ribosomal subunits (P protein). (B) 254nm absorbance tracing of control and stroke gradient samples. Dotted squares indicate respective monosome (80S) peaks. (C) Annotated transcript distributions of RPF tags in sham, control and stroke conditions. (D-E) Normalized coverage of ribosome profiling reads across all mRNAs for control and stroke, plotted as function of distance from (D) start and stop (E) codons. (F) EdgeR generated log2 CPM of genes identified by RPF (n=11,601) plotted against their log2 fold changes in stroke. Turquoise dots represent genes meeting a p-value cut-off of 0.01. All stroke samples collected after 3hr reperfusion following MCAO.

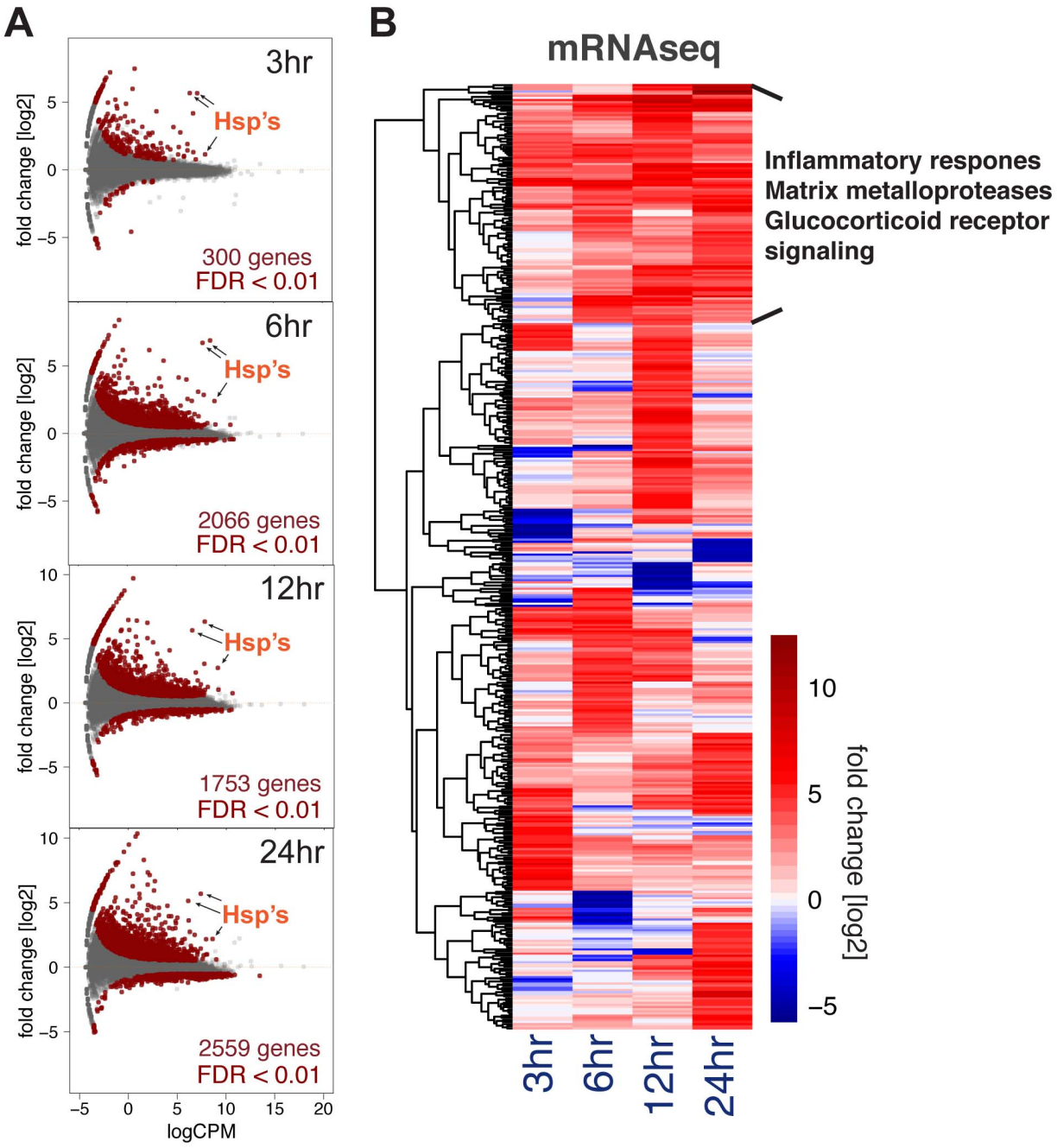

Supplementary Figure 4. Global characterization of mRNA expression at multiple reperfusion time points, related to Figure 4. (A) EdgeR generated log2 CPM RNAseq measures of RNA abundance for all expressed genes (n=22,340) plotted against their log2 fold changes in stroke, from top to bottom, 3, 6, 12, and 24hrs reperfusion following MCAO. Dark red dots indicate genes with significantly altered expression, FDR cut-off of 0.01. Genes coding for heat shock proteins marked by arrows for each time point. (B) Hierarchical clustering and heatmap visualization of differentially expressed mRNAs in stroke. Heatmap of log2 fold change values of 443 genes, with FDR cut-off of 0.01, and log2 fold change cut-off of |4|, for at least 1 out 4 time points. Red indicates up-regulated while blue is down-regulated. In brackets, top 3 pathway GOs enriched among genes of cluster representing predominantly up-regulated genes across all time points.

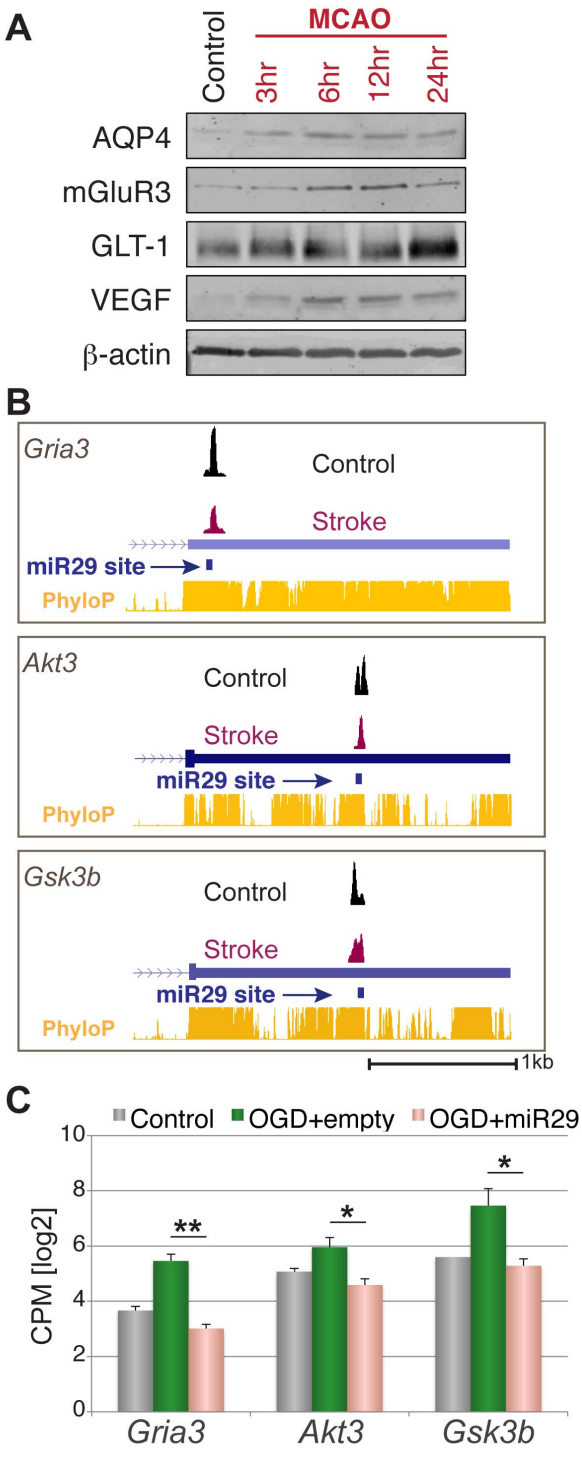

Supplementary Figure 5. Activated miR-29 targets in stroke, related to Figure 6. (A) Immunoblot analysis of total cortical protein collected from stroked animals at 3hr, 6hr, 12hr, and 24hr reperfusion times after MCAO, or from sham animals, β-actin serves as loading control. (B) Genome Browser views of miR-29 targets with corresponding CLIP peaks, similar to Figure 6C. (C) Normalized RNAseq [log2] CPM values of untreated control, OGD treated and infected with empty or miR-29 over-expression lenti-virus. *P<0.05, **P<0.005, Student's t test. Error bars represent ±SD.

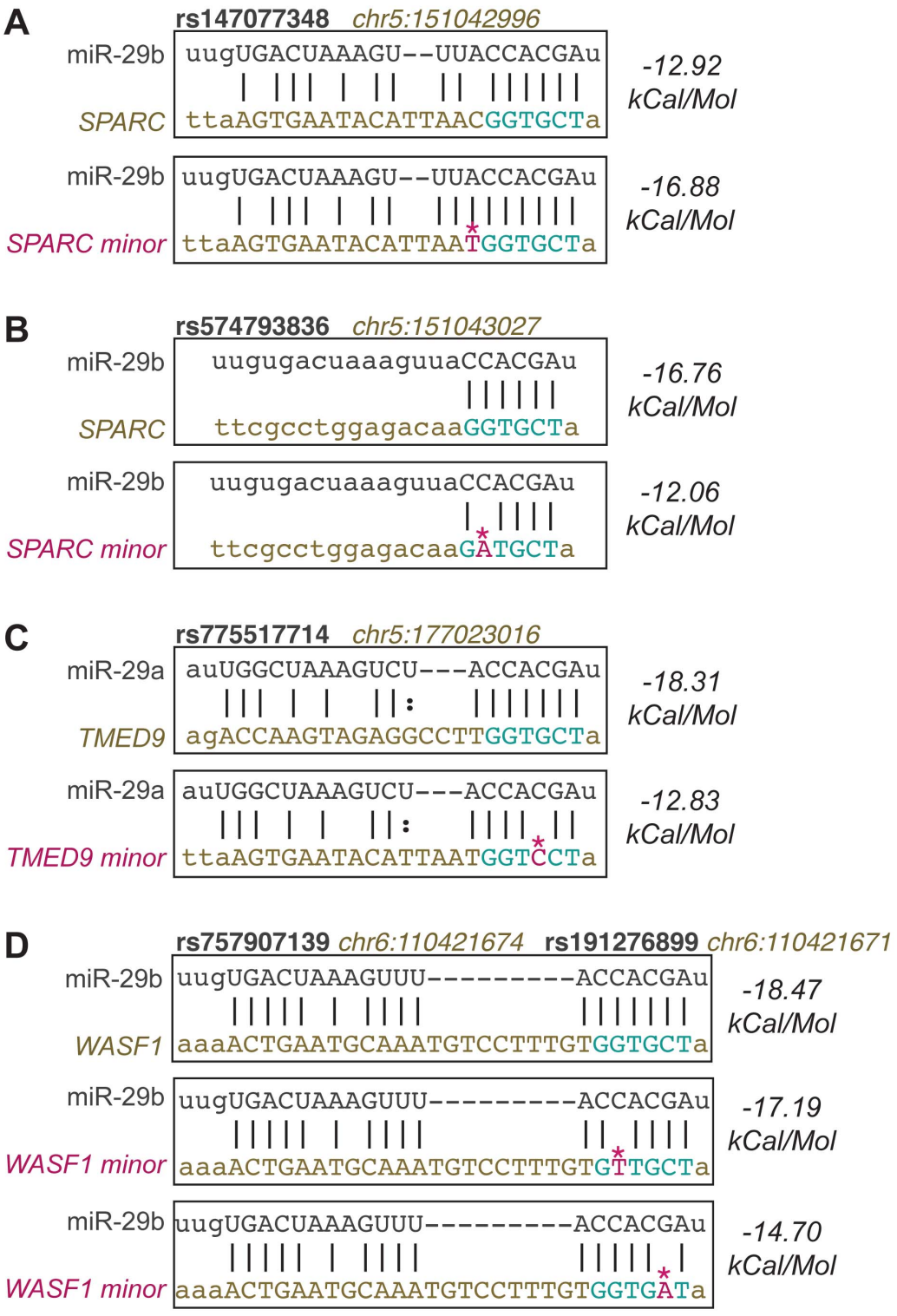

Supplementary Figure 6. Stroke relevant miR-29 binding site variants, related to Figure 7. Diagrams depicting differences in miR-29 family member pairing to stroke relevant binding sites for reference allele (top panels) and alternative allele (lower panels) for respective SNPs in (A-B) SPARC, (C) TMED9, and (D) WASF1 3'UTRs. Family member with most optimal pairing to target site reference sequence is shown. miRanda algorithm predicted binding energy coefficient for each pairing is indicated. Pink asterisk denote minor allele in seed sequence.

DATA AVAILABILITY

High-throughput sequencing data of AGO HITS-CLIP, RNAseq, miRNAseq and ribosomal profiling have been deposited to the NCBI Gene Expression Omnibus (GEO) under accession number GSE104053.

ACKNOWLEDGEMENTS

We thank R.B.Darnell and C.Iadecola lab members for invaluable suggestions, expertise, and feedback. Support was provided by the National Institutes of Health (NS034389, NS081706, NS097404, and 1UM1HG008901) to R.B.D, NS34179 to C.I., NS067078 to P.Z. Additional support was provided by the Simons Foundation (SFARI 240432) to R.B.D and Feil Family Foundation to C.I. R.B.D. is an Investigator of the Howard Hughes Medical Institute.

AUTHOR CONTRIBUTIONS

M.K., J.A., C.I., and R.B.D conceived the project. M.K. designed the studies and interpreted results. C.B. performed MCAo surgeries. C.A. performed OGD experiments. M.J.M provided mouse brain CLEAR-CLIP data. M.K. and A.M. generated AGO CLIP datasets. M.K. and J.J.F generated miRNAseq and RNAseq datasets. C.Y.P. ran miRANDA algorithm for SNPs. M.K. performed all other experiments, informatic analysis, and made figures. M.K. and R.B.D wrote the manuscript with input from all authors. R.B.D, C.I., J.A., and P.Z. supervised the research, and provided resources.

REFERENCES

1. Baek, D., Villén, J., Shin, C., Camargo, F.D., Gygi, S.P., and Bartel, D.P. (2008). The impact of microRNAs on protein output. Nature *455*, 64–71.

2. Bartel, D.P. (2009). MicroRNAs: Target Recognition and Regulatory Functions. Cell *136*, 215–233.

3. Bazzini AA, Lee MT, Giraldez AJ. (2012) Ribosome profiling shows that miR-430 reduces translation before causing mRNA decay in zebrafish. Science *336*, 233-7.

4. Benveniste H, Drejer J, Schousboe A, Diemer NH. (1984) Elevation of the extracellular concentrations of glutamate and aspartate in rat hippocampus during transient cerebral ischemia monitored by intracerebral microdialysis.
J Neurochem *43*, 1369-74.

5. Bilen, J., Liu, N., Burnett, B.G., Pittman, R.N., and Bonini, N.M. (2006). MicroRNA Pathways Modulate Polyglutamine-Induced Neurodegeneration. Mol. Cell *24*, 157–163.

6. Boudreau, R.L., Jiang, P., Gilmore, B.L., Spengler, R.M., Tirabassi, R., Nelson, J.A., Ross, C.A., Xing, Y., and Davidson, B.L. (2014) Transcriptome-wide Discovery of microRNA Binding Sites in Human Brain. Neuron *81*, 294–305.

7. Bracken, C.P., Li, X., Wright, J.A., Lawrence, D.M., Pillman, K.A., Salmanidis, M.,

Anderson, M.A., Dredge, B.K., Gregory, P.A., Tsykin, A., et al. (2014). Genome-wide identification of miR-200 targets reveals a regulatory network controlling cell invasion. Embo J. *33*, 2040–2056.

8. Brennecke, J., Stark, A., Russell, R.B., and Cohen, S.M. (2005). Principles of MicroRNA–Target Recognition. Plos Biol *3*, e85.

9. Brewster, B.L., Rossiello, F., French, J.D., Edwards, S.L., Wong, M., Wronski, A., Whiley, P., Waddell, N., Chen, X., Bove, B., et al. (2012). Identification of fifteen novel germline variants in the BRCA13′UTR reveals a variant in a breast cancer case that introduces a functional miR-103target site. Hum. Mutat. *33*, 1665–1675.

10. Broughton, J.P., Lovci, M.T., Huang, J.L., Yeo, G.W., and Pasquinelli, A.E. (2016). Pairing beyond the Seed Supports MicroRNA Targeting Specificity. Mol. Cell *64*, 320–333.

11. Buisson A, Choi DW. (1995) The inhibitory mGluR agonist, S-4-carboxy-3-hydroxy-phenylglycine selectively attenuates NMDA neurotoxicity and oxygen-glucose deprivation-induced neuronal death. Neuropharmacology. *34*, 1081–1087.

12. Chi, S.W., Zang, J.B., Mele, A., and Darnell, R.B. (2009). Argonaute HITS-CLIP decodes microRNA-mRNA interaction maps. Nature *460*, 479–486.

13. Chi SW, Hannon GJ, Darnell RB. (2012) An alternative mode of microRNA target recognition. Nat Struct Mol Biol *19*, 321-7.

14. Choi DW, Rothman SM. (1990) The role of glutamate neurotoxicity in hypoxic-ischemic neuronal death. Annu Rev Neurosci *13*, 171-82.

15. Davis, T.H., Cuellar, T.L., Koch, S.M., Barker, A.J., Harfe, B.D., McManus, M.T., and Ullian, E.M. (2008). Conditional Loss of Dicer Disrupts Cellular and Tissue Morphogenesis in the Cortex and Hippocampus. Journal of Neuroscience *28*, 4322–4330.

16. Delay C, Calon F, Mathews P, Hébert SS. (2011) Alzheimer-specific variants in the 3'UTR of Amyloid precursor protein affect microRNA function. Mol Neurodegener 6, 70.

17. Dharap, A., Bowen, K., Place, R., Li, L.-C., and Vemuganti, R. (2009). Transient Focal Ischemia Induces Extensive Temporal Changes in Rat Cerebral MicroRNAome. Journal of Cerebral Blood Flow & Metabolism *29*, 675–687.

18. Ebert MS, Sharp PA. (2012) Roles for microRNAs in conferring robustness to biological processes Cell *149*, 515-24.

19. Eichhorn, S.W., Guo, H., McGeary, S.E., Rodriguez-Mias, R.A., Shin, C., Baek, D., Hsu, S.-H., Ghoshal, K., Villén, J., and Bartel, D.P. (2014). mRNA Destabilization Is the Dominant Effect of Mammalian MicroRNAs by the Time Substantial Repression Ensues. Mol. Cell *56*, 104–115.

20. Flor PJ, Battaglia G, Nicoletti F, Gasparini F, Bruno V. (2002) Neuroprotective activity of metabotropic glutamate receptor ligands. Adv Exp Med Biol *513*, 197-223.

21. Fukuda AM, Badaut J. (2012) Aquaporin 4: a player in cerebral edema and neuroinflammation. J Neuroinflammation *9*, 279.

22. Grimson, A., Farh, K.K.-H., Johnston, W.K., Garrett-Engele, P., Lim, L.P., and Bartel, D.P. (2007). MicroRNA Targeting Specificity in Mammals: Determinants beyond Seed Pairing. Mol. Cell *27*, 91–105.

22. Grosswendt, S., Filipchyk, A., Manzano, M., Klironomos, F., Schilling, M., Herzog, M., Gottwein, E., and Rajewsky, N. (2014). Unambiguous Identification of miRNA:Target Site Interactions by Different Types of Ligation Reactions. Mol. Cell *54*, 1042–1054.

23. Guo, H., Ingolia, N.T., Weissman, J.S., and Bartel, D.P. (2010). Mammalian microRNAs predominantly act to decrease target mRNA levels. Nature *466*, 835–840.

24. Harvey BK, Airavaara M, Hinzman J, Wires EM, Chiocco MJ, Howard DB, Shen H, Gerhardt G, Hoffer BJ, Wang Y. (2011) Targeted over-expression of glutamate transporter 1 (GLT-1) reduces ischemic brain injury in a rat model of stroke. PLoS One 6, e22135.

25. Hébert SS, Horré K, Nicolaï L, Papadopoulou AS, Mandemakers W, Silahtaroglu AN, Kauppinen S, Delacourte A, De Strooper B. (2008) Loss of microRNA cluster miR-29a/b-1 in sporadic Alzheimer's disease correlates with increased BACE1/beta-secretase expression. Proc Natl Acad Sci U S A *105*, 6415-20.

26. Helwak, A., Kudla, G., Dudnakova, T., and Tollervey, D. (2013). Mapping the Human miRNA Interactome by CLASH Reveals Frequent Noncanonical Binding. Cell *153*, 654–665.

27. Ingolia NT, Ghaemmaghami S, Newman JR, Weissman JS. (2009) Genome-wide analysis in vivo of translation with nucleotide resolution using ribosome profiling. Science *324*, 218-23.

28. Jackman, K., Kunz, A., and Iadecola, C. (2011). Modeling Focal Cerebral Ischemia In Vivo. In Methods in Molecular Biology, (Totowa, NJ: Humana Press), pp. 195–209.

29. Jeyaseelan, K., Lim, K.Y., and Armugam, A. (2008). MicroRNA expression in the blood and brain of rats subjected to transient focal ischemia by middle cerebral artery occlusion. Stroke *39*, 959–966.

30. Johnson R, Zuccato C, Belyaev ND, Guest DJ, Cattaneo E, Buckley NJ. (2008) A microRNA-based gene dysregulation pathway in Huntington's disease. Neurobiol Dis *29*, 438-45.

31. Jung, H., Yoon, B.C., and Holt, C.E. (2012). Axonal mRNA localization and local protein synthesis in nervous system assembly, maintenance and repair. Nat Rev Neurosci.

32. Kalogeris T, Baines CP, Krenz M, Korthuis RJ. (2012) Cell biology of ischemia/

reperfusion injury. Int Rev Cell Mol Biol *298*, 229-317.

33. Khanna, S., Rink, C., Ghoorkhanian, R., Gnyawali, S., Heigel, M., Wijesinghe, D.S., Chalfant, C.E., Chan, Y.C., Banerjee, J., Huang, Y., et al. (2013). Loss of miR-29b following acute ischemic stroke contributes to neural cell death and infarct size. J Cereb Blood Flow Metab *33*, 1197–1206.

34. Kim, J., Inoue, K., Ishii, J., Vanti, W.B., Voronov, S.V., Murchison, E., Hannon, G., and Abeliovich, A. (2007). A MicroRNA Feedback Circuit in Midbrain Dopamine Neurons. Science *317*, 1220–1224.

35. Kingston AE, O'Neill MJ, Lam A, Bales KR, Monn JA, Schoepp DD. (1999) Neuroprotection by metabotropic glutamate receptor glutamate receptor agonists: LY354740, LY379268 and LY389795. Eur J Pharmacol. 377, 155-65.

36. Kozomara, A., and Griffiths-Jones, S. (2010). miRBase: integrating microRNA annotation and deep-sequencing data. Nucleic Acids Research *39*, D152–D157.

37. Kunz, A., Park, L., Abe, T., Gallo, E. F., Anrather, J., Zhou, P., and Iadecola, C. (2007) Neurovascular protection by ischemic tolerance: role of nitric oxide and reactive oxygen species. J Neurosci *27*, 7083–7093

38. Lal A, Navarro F, Maher CA, Maliszewski LE, Yan N, O'Day E, Chowdhury D, Dykxhoorn DM, Tsai P, Hofmann O, Becker KG, Gorospe M, Hide W, Lieberman J. (2009) miR-24 inhibits cell proliferation by targeting E2F2, MYC, and other cell-cycle genes via binding to "seedless" 3'UTR microRNA recognition elements. *Mol Cell* 35, 610-25.

39. Leung AK, Sharp PA. (2006) Function and localization of microRNAs in mammalian cells. Cold Spring Harb Symp Quant Biol *71*, 29-38.

40. Lewis, B.P., Burge, C.B., and Bartel, D.P. (2005). Conserved Seed Pairing, Often Flanked by Adenosines, Indicates that Thousands of Human Genes are MicroRNA Targets. Cell *120*, 15–20.

41. Licatalosi, D.D., Mele, A., Fak, J.J., Ule, J., Kayikci, M., Chi, S.W., Clark, T.A., Schweitzer, A.C., Blume, J.E., Wang, X., et al. (2008). HITS-CLIP yields genome-wide insights into brain alternative RNA processing. Nature *456*, 464–469.

42. Liu, C., Zhao, L., Han, S., Li, J., and Li, D. (2015). Identification and Functional Analysis of MicroRNAs in Mice following Focal Cerebral Ischemia Injury. Ijms *16*, 24302–24318.

43. Liu, D.-Z., Tian, Y., Ander, B.P., Xu, H., Stamova, B.S., Zhan, X., Turner, R.J., Jickling, G., and Sharp, F.R. (2009). Brain and blood microRNA expression profiling of ischemic stroke, intracerebral hemorrhage, and kainate seizures. Journal of Cerebral Blood Flow &Amp; Metabolism *30*, 92–101.

44. Loeb GB, Khan AA, Canner D, Hiatt JB, Shendure J, Darnell RB, Leslie CS, Rudensky AY. (2012) Transcriptome-wide miR-155 binding map reveals widespread noncanonical microRNA targeting. Mol Cell. *48*, 760-70.

45. Luna, J.M., Scheel, T.K.H., Danino, T., Shaw, K.S., Mele, A., Fak, J.J., Nishiuchi, E., Takacs, C.N., Catanese, M.T., de Jong, Y.P., et al. (2015). Hepatitis C Virus RNA Functionally Sequesters miR-122. Cell *160*, 1099–1110.

46. Maragakis, N.J., Dietrich, J., Wong, V., Xue, H., Mayer-Proschel, M., Rao, M.S., and Rothstein, J.D. (2004). Glutamate transporter expression and function in human glial progenitors. Glia *45*, 133–143.

47. Minones-Moyano, E., Porta, S., Escaramis, G., Rabionet, R., Iraola, S., Kagerbauer, B., Espinosa-Parrilla, Y., Ferrer, I., Estivill, X., and Marti, E. (2011). MicroRNA profiling of Parkinson's disease brains identifies early downregulation of miR-34b/c which modulate mitochondrial function. Human Molecular Genetics *20*, 3067–3078.

48. Moore, M.J., Scheel, T.K.H., Luna, J.M., Park, C.Y., Fak, J.J., Nishiuchi, E., Rice, C.M., and Darnell, R.B. (2015). miRNA–target chimeras reveal miRNA 3′-end pairing as a major determinant of Argonaute target specificity. Nat Comms *6*, 8864.

49. Moore, M.J., Zhang, C., Gantman, E.C., Mele, A., Darnell, J.C., and Darnell, R.B. (2014). Mapping Argonaute and conventional RNA-binding protein interactions with RNA at single-nucleotide resolution using HITS-CLIP and CIMS analysis. Nature Protocols *9*, 263–293.

50. Ouyang, Y.-B., Lu, Y., Yue, S., and Giffard, R.G. (2012). miR-181 targets multiple Bcl-2 family members and influences apoptosis and mitochondrial function in astrocytes. Mitochondrion *12*, 213–219.

51. Pandi, G., Nakka, V.P., Dharap, A., Roopra, A., and Vemuganti, R. (2013). MicroRNA miR-29c Down-Regulation Leading to De-Repression of Its Target DNA Methyltransferase 3a Promotes Ischemic Brain Damage. PLoS ONE *8*, e58039.

52. Riley, K.J., Rabinowitz, G.S., Yario, T.A., Luna, J.M., Darnell, R.B., and Steitz, J.A. (2012). EBV and human microRNAs co-target oncogenic and apoptotic viral and human genes during latency. Embo J. *31*, 2207–2221.

53. Rishal, I., and Fainzilber, M. (2013). Axon–soma communication in neuronal injury. Nat Rev Neurosci *15*, 32–42.

54. Roshan R, Ghosh T, Gadgil M, Pillai B. (2012) Regulation of BACE1 by miR-29a/b in a cellular model of Spinocerebellar Ataxia 17. RNA Biol *9*, 891-9.

55. Scheel, T.K.H., Luna, J.M., Liniger, M., Nishiuchi, E., Rozen-Gagnon, K., Shlomai, A., Auray, G., Gerber, M., Fak, J., Keller, I., et al. (2016). A Broad RNA Virus Survey Reveals Both miRNA Dependence and Functional Sequestration. Cell Host and Microbe *19*, 409–

56. Sepramaniam, S., Armugam, A., Lim, K.Y., Karolina, D.-S., Swaminathan, P., Tan, J.-R., and Jeyaseelan, K. (2010). MicroRNA 320a Functions as a Novel Endogenous Modulator of Aquaporins 1 and 4 as Well as a Potential Therapeutic Target in Cerebral Ischemia. Journal of Biological Chemistry *285*, 29223–29230.

57. Shioya, M., Obayashi, S., Tabunoki, H., Arima, K., Saito, Y., Ishida, T., and Satoh, J. (2010). Aberrant microRNA expression in the brains of neurodegenerative diseases: miR-

29a decreased in Alzheimer disease brains targets neurone navigator 3. Neuropathology and Applied Neurobiology *36*, 320–330.

58. Smirnova, L., Gräfe, A., Seiler, A., Schumacher, S., Nitsch, R., and Wulczyn, F.G. (2005). Regulation of miRNA expression during neural cell specification. Eur J Neurosci *21*, 1469–1477.

59. Tasca, C.I., Dal-Cim, T., and Cimarosti, H. (2014). In Vitro Oxygen-Glucose Deprivation to Study Ischemic Cell Death. In Methods in Molecular Biology, (New York, NY: Springer New York), pp. 197–210.

60. Verrier, J.D., Lau, P., Hudson, L., Murashov, A.K., Renne, R., and Notterpek, L. (2009). Peripheral myelin protein 22 is regulated post-transcriptionally by miRNA-29a. Glia *57*, 1265–1279.

61. Wang, Y., Huang, J., Ma, Y., Tang, G., Liu, Y., Chen, X., Zhang, Z., Zeng, L., Wang, Y., Ouyang, Y.-B., et al. (2015). MicroRNA-29b is a Therapeutic Target in Cerebral Ischemia Associated with Aquaporin 4. Journal of Cerebral Blood Flow; Metabolism *35*, 1977–1984.

62. Yuan Y, Wang JY, Xu LY, Cai R, Chen Z, Luo BY. (2010) MicroRNA expression changes in the hippocampi of rats subjected to global ischemia. J Clin Neurosci. *17*, 774–8.

63. Zhang, Y., Chen, K., Sloan, S.A., Bennett, M.L., Scholze, A.R., O'Keeffe, S., Phatnani, H.P., Guarnieri, P., Caneda, C., Ruderisch, N., et al. (2014). An RNA-Sequencing Transcriptome and Splicing Database of Glia, Neurons, and Vascular Cells of the Cerebral Cortex. Journal of Neuroscience *34*, 11929–11947.

64. Zhang L, Dong L, Li Y, Hong Z, Wei W (2012) The microRNA miR-181c controls microglia-mediated neuronal apoptosis by suppressing tumor necrosis factor. J Neuroinflammation *9*, 211.

65. Zhao X, Ye Q, Xu K, Cheng J, Gao Y, Li Q, Du J, Shi H, Zhou L. (2013) Single-nucleotide polymorphisms inside microRNA target sites influence the susceptibility to type 2 diabetes. Hum Genet *58*, 135-41.

SUPPLEMENTAL REFERENCES

1. Betel D, Wilson M, Gabow A, Marks DS, Sander C. (2008) The microRNA.org resource: targets and expression. Nucleic Acids Res *36(Database issue)*, D149-53

2. Cahoy JD, Emery B, Kaushal A, Foo LC, Zamanian JL, Christopherson KS, Xing Y, Lubischer JL, Krieg PA, Krupenko SA, Thompson WJ, Barres BA. (2008) A transcriptome database for astrocytes, neurons, and oligodendrocytes: a new resource for understanding brain development and function. J Neurosci *28*, 264-78.

3. Dobin A, Davis CA, Schlesinger F, Drenkow J, Zaleski C, Jha S, Batut P, Chaisson M, Gingeras TR. (2013)STAR: ultrafast universal RNA-seq aligner. Bioinformatics *29*, 15-21.

4. Goecks J, Nekrutenko A, Taylor J, Galaxy Team. (2010) Galaxy: a comprehensive approach for supporting accessible, reproducible, and transparent computational research in the life sciences. Genome Biol *11*, R86.

5. Ihaka R, Gentleman R. (1996) R: a language for data analysis and graphics. J Comput Graph Stat *5*, 299–314.

6. Kent, W.J., Sugnet, C.W., Furey, T.S., Roskin, K.M., Pringle, T.H., Zahler, A.M., and Haussler, D. (2002). The human genome browser at UCSC. Genome Res. *12*, 996–1006.

7. Langmead B, Salzberg SL. (2012) Fast gapped-read alignment with Bowtie 2. Nat Methods *9*, 357-9

8. Nelson PT, De Planell-Saguer M, Lamprinaki S, Kiriakidou M, Zhang P, O'Doherty U, Mourelatos Z. (2007) A novel monoclonal antibody against human Argonaute proteins reveals unexpected characteristics of miRNAs in human blood cells. RNA *13*,1787-92.

9. Robinson MD, McCarthy DJ, Smyth GK. (2010) edgeR: a Bioconductor package for differential expression analysis of digital gene expression data. Bioinformatics 26, 139-40.

10. Weyn-Vanhentenryck SM, Mele A, Yan Q, Sun S, Farny N, Zhang Z, Xue C, Herre M, Silver PA, Zhang MQ, Krainer AR, Darnell RB, Zhang C. (2014) HITS-CLIP and integrative modeling define the Rbfox splicing-regulatory network linked to brain development and autism. Cell Rep *6*, 1139-52.